



Wellbore Trajectory Optimization of an Iranian Oilfield Based on Mud Pressure and Failure Zone

H. Yousefian¹, M. Fatehi Marji^{2*}, H. Soltanian¹, A. Abaollahipour³, Y. Pourmazahri¹

1. Drilling & Well Completion Technologies & Research Group, Research Institution of Petroleum Industry (RIPI), Tehran, Iran

2. Department of Mining and Metallurgical Engineering, Yazd University, Yazd, Iran

3. School of Mining Engineering, College of Engineering, University of Tehran, Tehran, Iran

Received 12 August 2019; received in revised form 16 September 2019; accepted 10 January 2020

Keywords

Borehole breakout

Well trajectory

Failure zone

Critical pressure

Induced stress

Abstract

Determination of the borehole and fracture initiation positions is the main aim of a borehole stability analysis. A wellbore trajectory optimization with the help of the mud pressure may be unreasonable since the mud pressure can only reflect the degree of difficulty for the initial damage to occur at the wellbore rather than the extent of the wellbore damage. In this work, we investigate the failure extension in different arbitrary inclination boreholes under different in-situ stress regimes. Assuming the plane strain condition, the Mohr-Coulomb, Mogi-Coulomb, and Modified Lade rock failure criteria are utilized. We present an analytical equation to determine the optimum drilling trajectory of an Iranian oilfield. In order to predict the degree of wellbore damage, the initial shear failure location, failure width, and failure depth of arbitrary wellbores are determined. Then a new model is derived to calculate the initial failure area of a directional wellbore because it is more efficient in a wellbore stability analysis. The results obtained show that in the target oilfield, the vertical and low-deviated direction is the optimum drilling path. According to the results of this work, optimization of the wellbore trajectory based on the estimated failure zone is a reasonable method if a considerable failure zone takes place around the borehole wall.

1. Introduction

The stability of oil and gas wells is completely affected by the *in-situ* stress system of the oil and gas fields. When a well is drilled, the rock medium surrounding the borehole experiences a stress concentration previously taken by the removed rock [1]. As a result, the induced stresses around the borehole wall change significantly. In fact, this increases the magnitude of the induced stresses and creates a stress concentration around the borehole wall. If the stress concentration exceeds the strength of the surrounded rock, a failure zone will be formed around the borehole wall, leading to instability problems for a drilling operation [2, 3]. Moreover, multiple groups of weak planes are known as the main factors of wellbore instability in the shale formation; these weak planes affect the stress distribution and shale strength. Hence, the

collapse pressure increases with increase in the anisotropy of shale formation. Additionally, different occurrences and numbers of weak planes cause variation in the collapse pressure [4-6].

Drilling operations show that a shear failure will take place when the mud pressure decreases to a value known as the critical or failure pressure [7]. Therefore, in order to avoid the occurrence of any damage zone around the borehole wall, the mud pressure must be increased [8]. On the other hand, an increase in the mud pressure may cause induced tensile fractures around the borehole wall in some situations [9-12]. The drilling engineers try to design a safe mud window in order to decrease the impact of stress concentration and prevent the formation of any failure zone around the borehole wall [13-17]. In addition, the existence of a slight

✉ Corresponding author: mfatehi@yazd.ac.ir (M. Fatehi Marji).

amount of failure zone around the borehole wall does not always lead to the instability of wellbores. Thus the mud pressure can be lower than the critical pressure in some situations during a drilling operation [9]. Moreover, the wellbore stability studies show that the critical pressure cannot be a suitable and economical factor involved for optimization of the mud pressure because the critical pressure can only indicate the potential of failure zone formation around the borehole wall. Therefore, it is unable to predict the degree of failure zone [9]. Formation of the failure zone can also be used as a key factor to investigate the variation in porosity and permeability of the formations surrounding the borehole and its impact on the production rate [18]. Actually, the numerical simulation of slabbing near the borehole wall could propose an accurate prediction of the fracture zone around this region [17, 19-22]. Furthermore, Adnoy and Kaarsta have shown that the extension degree of the failure zone can be estimated from the rock mechanics properties and *in-situ* stresses of the target formation. It is a good idea to optimize the wellbore trajectory and design a safe mud window based on these factors [23]. Following this procedure, Quang Li and Tang have optimized the trajectory of a wellbore using the extension degree of the failure zone [10]. Zhiyue Wang and Deli Gao have presented a mathematical formulation for a deviation-correction trajectory design in the case of an undetermined target point, and an optimum design model has been established to consider two cases of planned trajectory [24]. Weidong Zhang *et al.* have proposed a series of new equations during which, optimization of the well trajectory has been conducted based on the position of the failure zone around the borehole wall in different *in-situ* stress regimes [25]. Atashnezhad *et al.*, in an attempt to develop optimization of the well trajectory, have introduced a new stochastic approach for a drilling trajectory design, applying the continuous particle swarm algorithms to find the optimum drilling measured depth of directional and horizontal wells in a 3D space [26]. Also Ethar Alkamil *et al.* have analyzed the stability of several wells in an oilfield in Iraq. They compiled a 1D mechanical earth model (MEM) of the Mishrif formation based on its state of stress and rock strength parameters. This model assesses the contribution of borehole collapse leading to the stuck pipe problems. Finally, feasible drilling trajectories have been determined with respect to the Mohr-Coulomb, Mogi-Coulomb, and Modified Lade rock failure criteria [27].

In order to investigate the optimum and stable drilling path of an oilfield in SW of Iran, this paper proposes an analytical model utilizing a linear elastoplastic theory and a shear failure criterion. This model is capable of offering an optimized stable drilling path in the isotropic and homogeneous condition in the target oilfield. The main aim of this work was to suggest the initial plane of the optimized drilling trajectory in the target oilfield. The optimum well path was determined based on four factors including the minimum and maximum mud pressure, relative failure area, and wide extension of the failure zone. As mentioned, in this work, we just estimate the potential occurrence of the failure zone and its expansion rate in different orientations.

2. Methodology

2.1. Borehole stresses of deviated well

As mentioned earlier, the drilling process causes a stress concentration around the borehole wall. Therefore, selecting the optimum drilling path requires investigation of the induced stress condition around the borehole wall in different orientations. In order to estimate the induced stress of one arbitrarily inclined borehole, the stress tensor must be translated from the global *in-situ* coordinate system (x',y',z') to a local borehole coordinate system (x,y,z). As shown in Figure 1, this transformation is according to the Euler angles [28, 29].

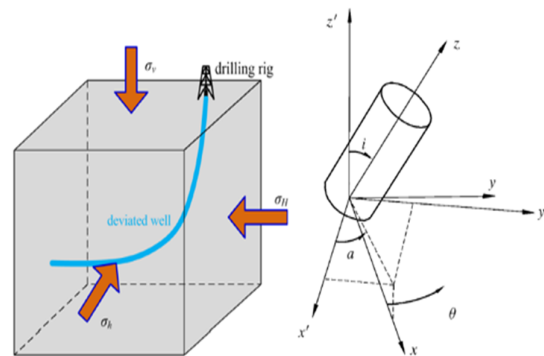


Figure 1. Coordinate system for a deviated borehole.

After transferring the stress tensor to the local borehole coordinate system, the stress concentration around the borehole wall must be computed. According to the homogeneous linear elastic model, the borehole wall stresses can be calculated in the term of the radial function, which is known as the Kirsch solution [28].

The borehole wall stresses must be substituted in the intended failure criterion. Therefore, as given below, the main stress must be computed [29].

$$\sigma_{1,2} = \frac{1}{2}(\sigma_{\theta\theta} + \sigma_{zz}) \pm \frac{1}{2}\sqrt{(\sigma_{\theta\theta} - \sigma_{zz})^2 + 4\tau_{\theta z}^2} \quad (1)$$

$$\sigma_3 = \sigma_{rr}$$

In order to calculate the borehole wall stresses in all orientations, the dip and dip directions were varied in the range of 0°-90° and 0°-360°, respectively (Figure 1). A tensile fracture take place when the least effective principle stress around the borehole wall exceeds the tensile strength of the rock:

$$\sigma_2 - \alpha P_p = -S_t \quad (2)$$

where α is the Biot constant. By substituting σ_2 in Eq. (1) in Eq. (2), the tensile fracture pressure can be determined as below:

$$P_{wf} = \sigma_x + \sigma_y - 2(\sigma_x - \sigma_y)\cos 2\theta - 4\tau_{xy}\sin 2\theta - \frac{\tau_{\theta z}^2}{\sigma_z + S_t - \alpha P_p} + S_t - \alpha P_p \quad (3)$$

The first derivative of Eq. (3) is taken with respect to θ and equated to zero in order to determine the position of the induced tensile fracture and borehole breakout around the borehole wall, i.e. $\partial P_{wf} / \partial \theta = 0$, given [25, 30, 31]:

$$\tan 2\theta = \frac{2\tau_{xy}(\sigma_z - P_p) - \tau_{xz}\tau_{zy}}{(\sigma_x - \sigma_y)(\sigma_z - P_p) - \tau_{xz}^2 - \tau_{yz}^2} \quad (4)$$

Since the normal stresses are much larger than the shear stresses, the second order of shear stresses can be neglected. Thus the general analytical equation for use to predict the position of the induced tensile fracture and borehole breakout is given as below:

$$\theta = \frac{1}{2} \tan^{-1} \frac{\tau_{xy}}{\sigma_{xx} - \sigma_{yy}} \quad (5)$$

$$\theta_{\text{induce-tensile-fracture}} = \theta$$

$$\theta_{\text{breakout}} = \theta + 90$$

According to Eq. (5), the position of formation of borehole breakout differs by 90° from the position of the induced tensile fracture [9, 28].

2.2. Compressive failure criteria

The compressive failure criteria may be divided into two categories based on considering or

ignoring the effect of the intermediate principal stress. The failure criteria such as the Mohr-Coulomb criterion ignore the influence of the intermediate principal stress on the strength ($\sigma_1 > \sigma_2 = \sigma_3$). These compressive failure criteria are conservative. However, the Mohr-Coulomb criterion is common in the petroleum industry due to its simplicity. Another group of failure criteria considers the effect of the intermediate principal stress. Therefore, a better estimation of the failure zone around the borehole wall has been proposed. Mogi-Coulomb and modified Lade are examples of these criteria [9, 32, 33].

In this work, we decided to use the Mohr-Coulomb, Mogi-Coulomb, and modified Lade criteria to analyze the status of the failure zone around the borehole wall.

2.2.1. Mohr-Coulomb criterion

Mohr-Coulomb is one of the most commonly used failure criteria in geomechanics with a simple linear form. According to this criterion, rock failure will occur in the direction of a plane due to the shear stress acting on that plane. The normal stress components, internal cohesion of rock, and a frictional force act against the shear stress on the plane of failure. In this criterion, $f(\sigma)$ as a linear function of σ , is defined as [32, 33]:

$$(\sigma_1) = \sigma_c + (\sigma_3)\tan^2 \beta \quad (6)$$

$$\beta = \phi/2 + 45^\circ \quad (7)$$

where σ_c is the uniaxial compressive strength.

2.2.2. Mogi-Coulomb criterion

This criterion is the result of the true-triaxial experiments of Mogi (1971) on different rock types. Mogi pointed out that the mean normal stress that opposed the creation of fracture was σ_2 , rather than the octahedral normal stress σ_{oct} . Actually, he assumed that the distortional strain energy as a frictional force was proportional to the octahedral shear stress τ_{oct} and would be increased by increasing σ_2 until a critical level where a failure occurred. Based on these results, Al. Ajmi and Zimmerman (2005) proposed a linear relationship that could be written as Eqs. (8) to (10) [34, 35]:

$$\tau_{oct} = a + b\sigma_{m,2} \quad (8)$$

$$\tau_{oct} = \frac{1}{3} \sqrt{(\sigma_1 - \sigma_2)^2 + (\sigma_2 - \sigma_3)^2 + (\sigma_1 - \sigma_3)^2} \quad (9)$$

$$\sigma_{m,2} = \frac{\sigma_1 + \sigma_3}{2} \quad (10)$$

where a and b are the constants of the material, and can be calculated by C and φ .

$$a = \frac{2\sqrt{2}}{3} C \cos \varphi \quad (11)$$

$$b = \frac{2\sqrt{2}}{3} \sin \varphi \quad (12)$$

2.2.3. Modified Lade criterion

With reference to the experimental observations, Lade (1977) offered this criterion for a cohesion less soil. Lade believed that the frictional angle decreased with increase in the magnitude of mean normal stress. An original relationship which that was developed by Lade in terms of the first and the third stress invariants included the material constant and atmospheric pressure parameters. Also the stress invariant parameters I_1 and I_3 in the Lade criterion were not determined based on the effective stresses concept. In order to consider the impact of cohesion on the shear strength of the material, the original Lade criterion was modified by Ewy in 1998. The modified version that was developed based on an effective stress is given below [36, 37]:

$$\frac{I_1''}{I_3''} = 27 + \eta \quad (13)$$

$$I_1'' = (\sigma_1 + S) + (\sigma_2 + S) + (\sigma_3 + S) \quad (14)$$

$$I_3'' = (\sigma_1 + S)(\sigma_2 + S)(\sigma_3 + S) \quad (15)$$

where S and η are constants of the material, and can be calculated from:

$$S = \frac{C}{\tan \varphi} \quad (16)$$

$$\eta = \frac{4(\tan \varphi)^2 (9 + 7 \sin \varphi)}{1 - \sin \varphi} \quad (17)$$

2.3. Calculation of pressure of shear and tensile failure

2.3.1. Pressure of shear failure

According to the foregoing steps, the existence or absence of the failure zone around the borehole wall can be predicted by a failure criterion. Also the

pressure required to create this failure zone can be determined. Generally, the shear failure pressure is equal to the amount of mud pressure during which the concentration of borehole wall stresses exceeds the shear strength of the rock around the borehole wall. Hence, in order to assess this pressure, the mud pressure is considered unknown in the Kirsch equations. Then the principal induced stresses are computed using Eq. (1). After that, the principal calculated stresses are substituted in the mentioned failure criteria, and finally, the shear failure pressure is determined.

2.3.2. Pressure of induced tensile failure

As described earlier, when the minimum principal induced stress at the borehole wall exceeds the tensile strength of the rock, the induced tensile fracture will occur (Eq. (2)).

The tensile failure will take place when the minimum principal induced stress at the borehole wall exceeds the tensile strength of the rock media around the borehole wall. The tensile failure pressure can be computed by Eq. (3).

2.4. Evaluation of extension of failure zone around borehole wall

2.4.1. Assessing radius of failure zone

Most analytical methods consider the drilled rock formations as an elastic or a poroelastic medium, whereas in some conditions, the surrounding formations of borehole have a plastic behavior (Figure 2).

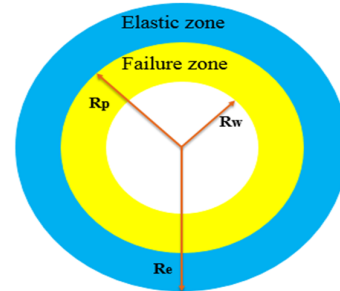


Figure 2. Failure zone around borehole wall.

Estimating the radius of the failure zone around the borehole wall is one of the most important topics in a plastic analysis. In order to assess the radius of the failure zone, the borehole wall stresses are substituted in the failure criterion. Then an equation in the term of r is derived. The radius of the failure zone (R_p) is estimated by solving this equation. In this method, it is assumed that the equation for each failure criterion consists of two parts. The term at the right hand side is the stable part, and the left one is the unstable part. If the

unstable part is greater than the stable part, the failure zone will happen. Wherever the unstable part and the stable part are equal, the intersection will represent the radius of the failure zone (Figure 2) [14].

Since the failure zone reaches its maximum value near the borehole breakout, all the mentioned processes for calculating the radius of the failure zone are conducted along the borehole breakout.

2.4.2. Assessing wide extension and relative area of failure zone

As shown in Figure 3, the failure zone is expected to be created in the symmetric form around the borehole wall and follow the elliptical shape. Also in the critical situation, this failure zone can cover all around the borehole. Therefore, in order to estimate the extension of the failure zone, all of the calculations are conducted in a quarter of the borehole section between the induced tensile fracture and the borehole breakout. During these calculations, in the first step, the borehole wall stresses are computed between the induced tensile fracture and the borehole breakout. Then they are substituted in the failure criterion, and wherever the unstable part and the stable part of the failure criterion are equal, the plastic zone starts to initiate. According to Figure 3, by detecting the initial point of the failure zone, the width extension of this zone can be determined as below:

$$\omega = (\theta_{ini} - \theta_B) \tag{18}$$

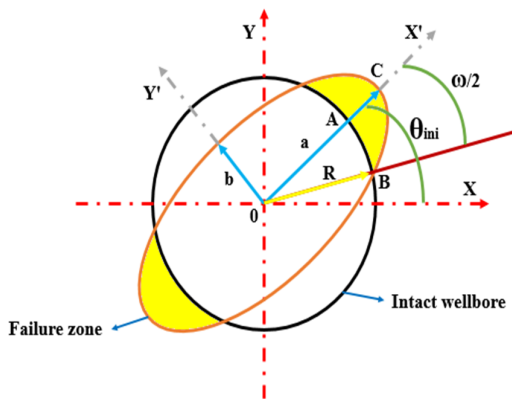


Figure 3. Initial shear failure of arbitrary wellbore.

As illustrated in Figure 3, the failure area equals the difference between the ellipse and the overlapping portions. Thus according to the process described, the short axis of the ellipse is the only required parameter that must be determined to estimate the

failure area. Using the relationship between the ellipse and the circle and combining the long semi-axis (a) and the wide extension of failure zone (ω), the short semi-axis (b) of the ellipse can be calculated as given below:

$$b = \begin{cases} r_{180} (\omega = 180) \\ \frac{aR \sin(\omega/2)}{\sqrt{a^2 - R^2 \cos(\omega/2)}} (0 < \omega < 180) \end{cases} \tag{19}$$

where r_{180} is the failure radius, and it takes place when the failure zone extends to the whole borehole. Having the short semi-axis (b) determined, the failure area can be computed as the difference between the ellipse sector area and the circle sector area along the failure portion. Regarding Figure 4, the ellipse sector area can be written as below:

$$A(\theta)_{ellipse} = \frac{1}{2} ab \tan^{-1} \left(\frac{a \tan(\theta)}{b} \right) \tag{20}$$

where a and b are the long semi-axis and short semi-axis ellipse, respectively, and θ is the angle of the selected sector in Figure 4.

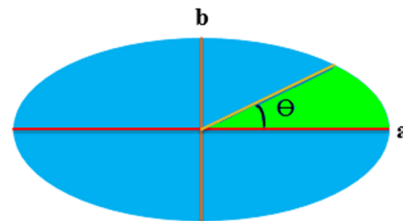


Figure 4. Ellipse sector area.

Now, the relative failure area is calculated by the following equation:

$$A_{failure} = [A(\omega)_{ellipse} - A(\omega)_{circle}] * 100 \tag{21}$$

2.5. Validation of proposed method

In this work, the stability of an arbitrary wellbore under different stress situations and specific rock mechanics properties are analyzed to verify the proposed method. For a more accurate validation, the stability of the mentioned wellbore is simulated in a particular direction by the finite difference numerical method. The *in-situ* stress regimes and rock properties of one well for sandstone rock at a vertical depth of 4500 m are shown in Table 1. The direction of maximum horizontal principal stress is NE0° [10].

Table 1. In-situ stress regime and rock properties of validation example [10].

Stress regime	Depth (m)	σ_v (MPa)	σ_H (MPa)	σ_h (MPa)	Pore pressure (MPa)	Well pressure (MPa)	σ_c (MPa)	Φ°	E (GPa)	ν
Normal		130.5	121.5	112.5						
Strike-slip	4500	121.5	130.5	112.5	72	72	67	30	10	0.25
Reverse		112.5	130.5	121.5						

According to Figures. 5 to 7, the variation in the four factors of minimum mud pressure, relative failure depth, width extension of failure zone, and relative failure area are presented for the normal, strike-slip, and inverse *in-situ* stress regime. All of these calculations are based on the Mohr-Coulomb, Mogi-Coulomb, and modified Lade criteria. The magnitude of each forenamed factors in different orientations is represented by using any special color. Red indicates a relatively unstable well, whereas blue indicates the opposite.

According to Figure 5, under the normal *in-situ* stress regime, the failure zone will take place with the most width extension and relative area in the horizontal or highly deviated boreholes ($\theta > 60^\circ$) along the minimum principal horizontal stress. Also for the horizontal or highly deviated ($\theta > 80^\circ$) boreholes, the relative failure depth and minimum mud pressure are in the critical situation. Thus with respect to the results of the three failure criteria, drilling the vertical or low deviated wells less than 45° is the most optimum drilling path.

In the strike-slip *in-situ* stress (Figure 6), the failure width reaches its maximum amount along the horizontal and highly deviated wells, while the critical amount of the relative failure area is limited to near the minimum principal horizontal stress. On the other hand, drilling the vertical, deviated, and horizontal wells along the minimum principal horizontal stress has a high relative failure depth and a critical minimum mud pressure. Accordingly, the vertical and low-deviated drilling paths less than 30° have a high failure depth and a critical minimum mud pressure, whereas the failure width and the relative failure area are minimized.

Under the reverse *in-situ* stress regime, the failure width and the relative failure area will take place in a high amount when drilled horizontally or with highly deviated wells along the maximum principal horizontal stress. For any arbitrary-deviated well along the minimum principal horizontal stress, the failure depth and the minimum mud pressure reach their maximum amounts. Thus the vertical and low-deviated drilling paths are determined as the poorly stable well trajectories (Figure 7).

Figure 8 presents the final shape of the failure zone in the worst situation of the three mentioned *in-situ* stress regimes. Due to the same stress regime and rock properties, the three *in-situ* stress regimes show similar failure zones. According to the Mohr-Coulomb, Mogi-Coulomb, and modified Lade criteria, the failure widths are 180° , 180° , and 131.6° , and the failure depths reach the maximum amounts of 1.32, 0.70, and 0.55 cm, respectively. Based on the Mogi-Coulomb criterion, the minimum failure depth is 0.07 cm in a limit of 50° near the borehole wall. As a result, the effective failure area reduces to the limit of 132° , approximately the same as the modified Lade criterion. On the other hand, these narrow failure zones are unable to make any special challenge in the wellbore stability and other geomchanics issues. Thus only the wide and deep failure zone could cause a challenge for the drilling operation.

Generally, it can be claimed that the minimum mud pressure, failure depth, failure width, and relative failure area may be used to predict the breakout. The results obtained may be categorized into two groups. Group A includes the minimum mud pressure and failure depth, and group B includes the failure width and the relative failure area. The results of the group A members are in more agreement as well as the results of group B for its members. Comparing groups A and B with the field data shows that the optimized orientation based on the minimum mud pressure and failure depth might be more conservative than the real situation, while the failure area and failure width have a more accuracy and present a more realistic prediction from the optimum well trajectory. The failure area is a result of the failure width, failure depth, and failure position. It is able to propose a better image of the failure zone in comparison with the failure depth and failure width. Therefore, it can analyze the instability of the arbitrary-deviated wellbore comprehensively. On the other hand, the failure area may be used as a helpful and effective parameter in the petroleum geomechanics studies such as sand production.

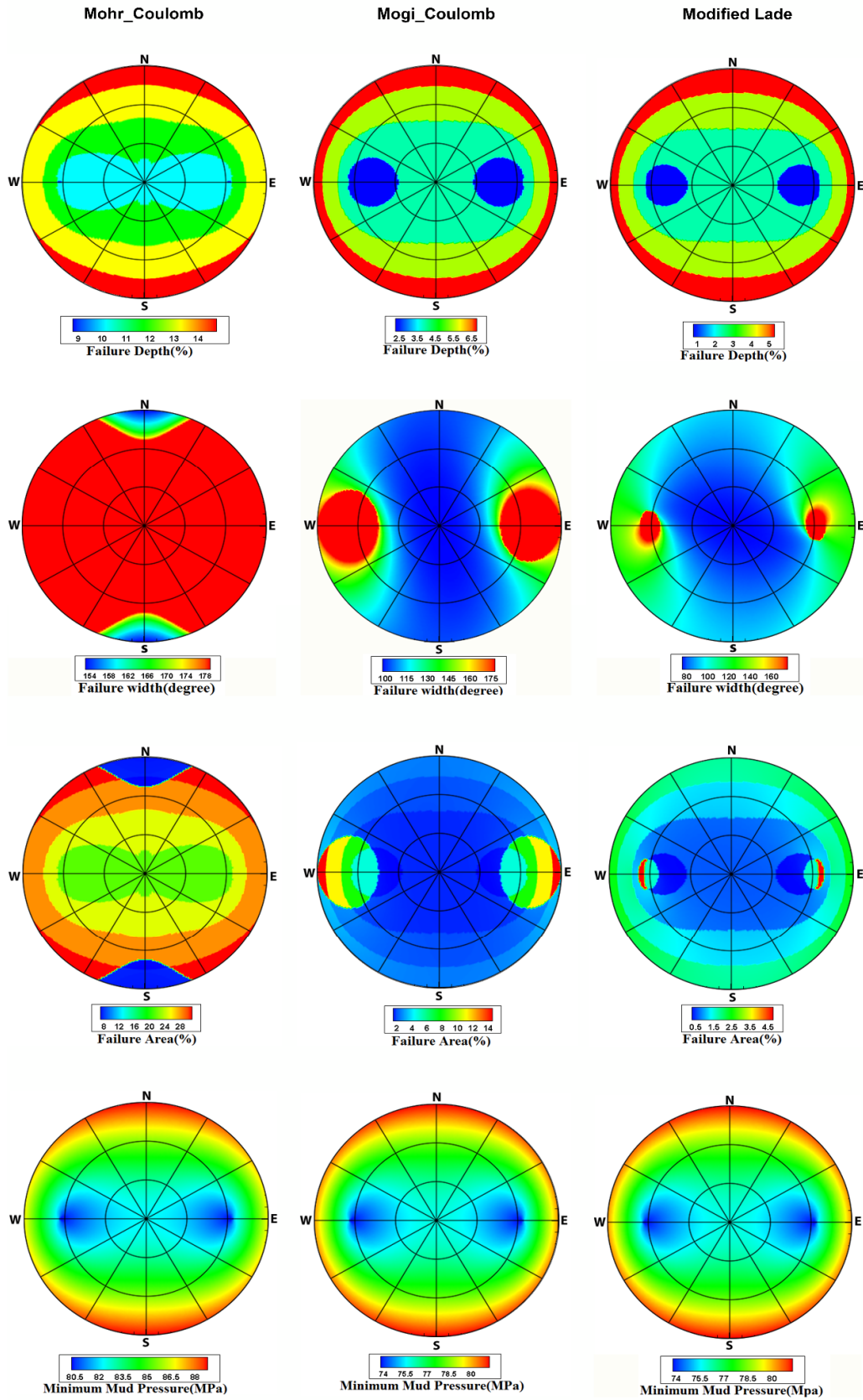


Figure 5. Stability of arbitrary wellbores under the normal *in-situ* stress regime.

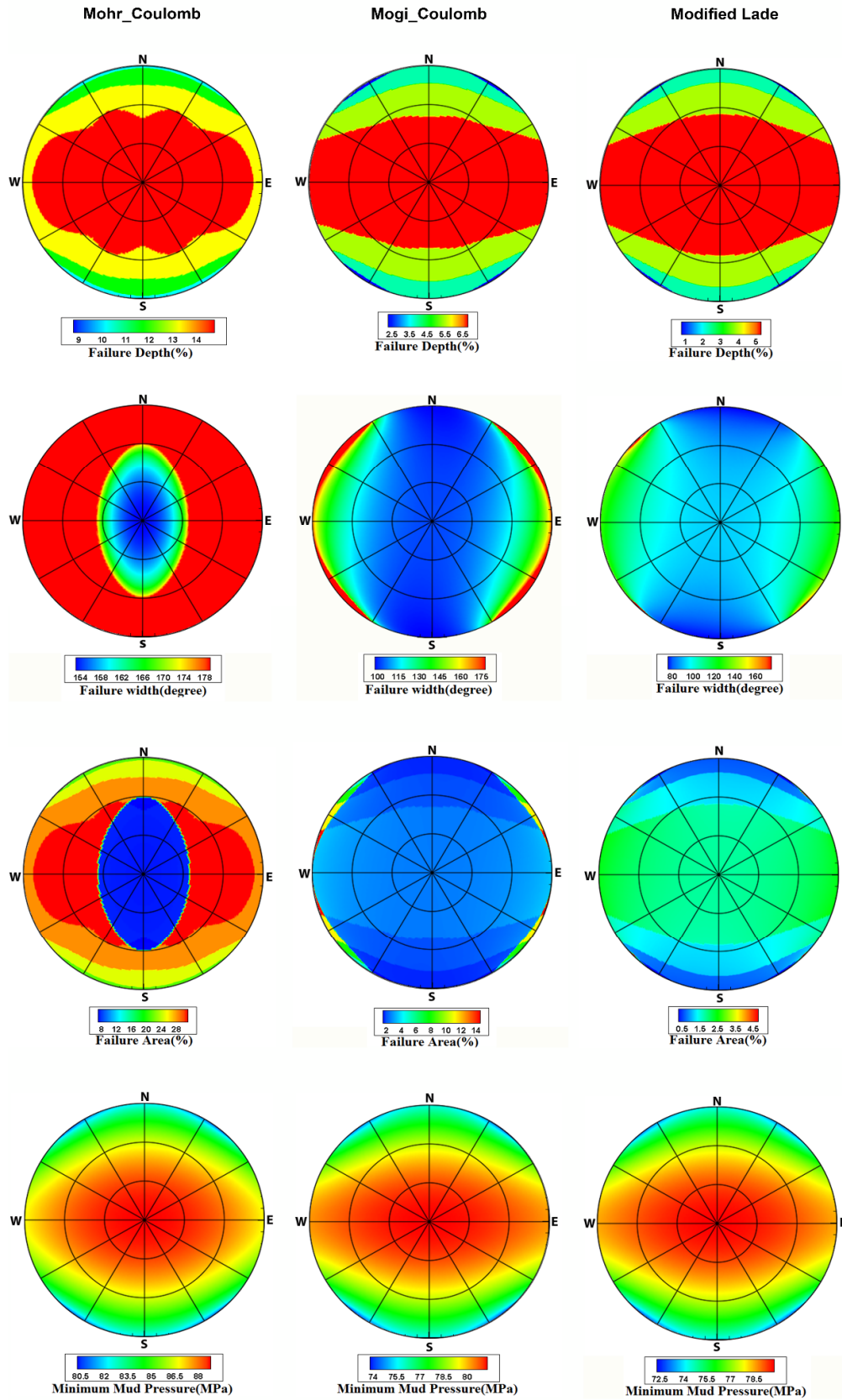


Figure 6. Stability of arbitrary wellbores under the strike slip *in-situ* stress regime.

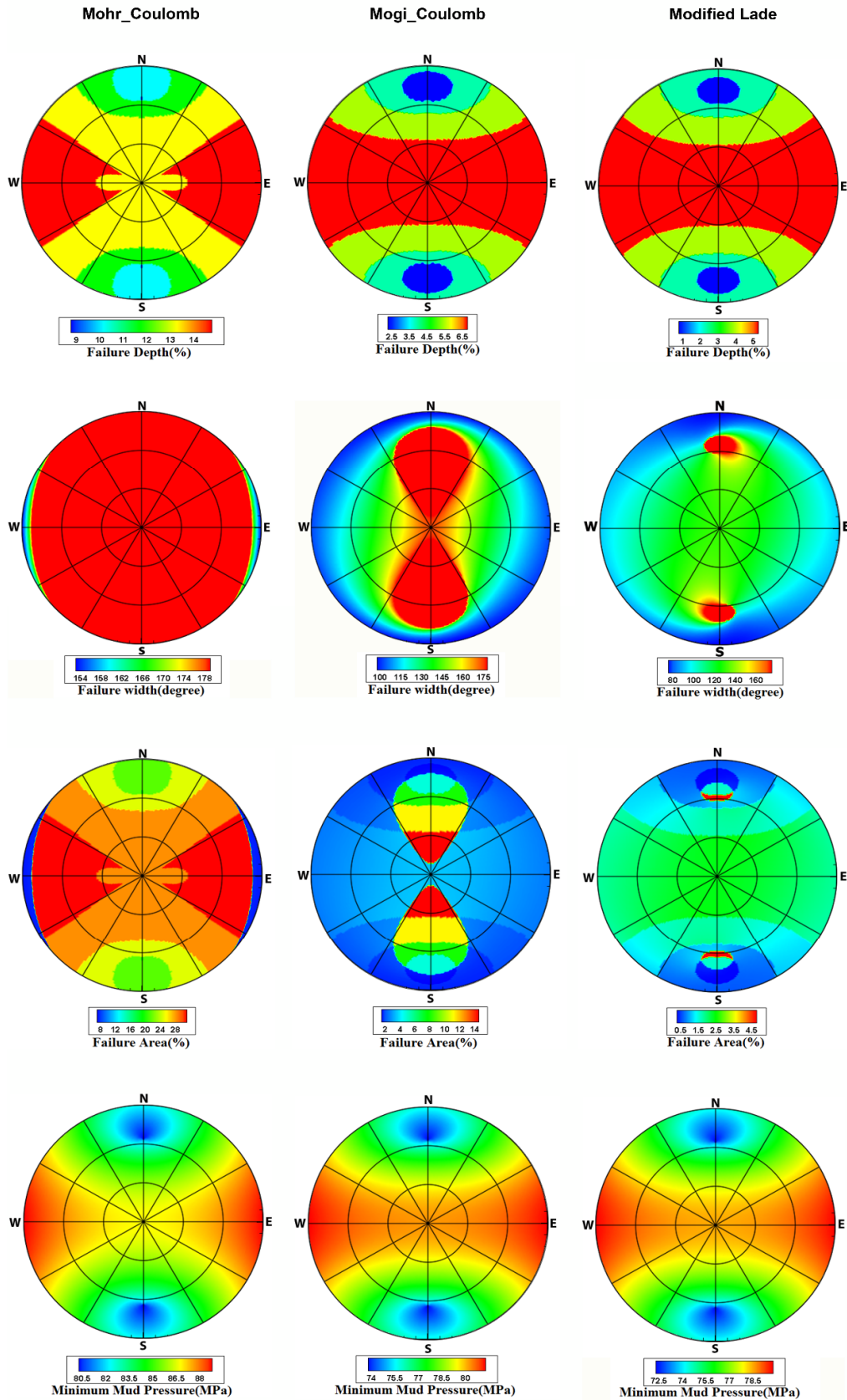


Figure 7. Stability of arbitrary wellbores under the reverse *in-situ* stress regime.

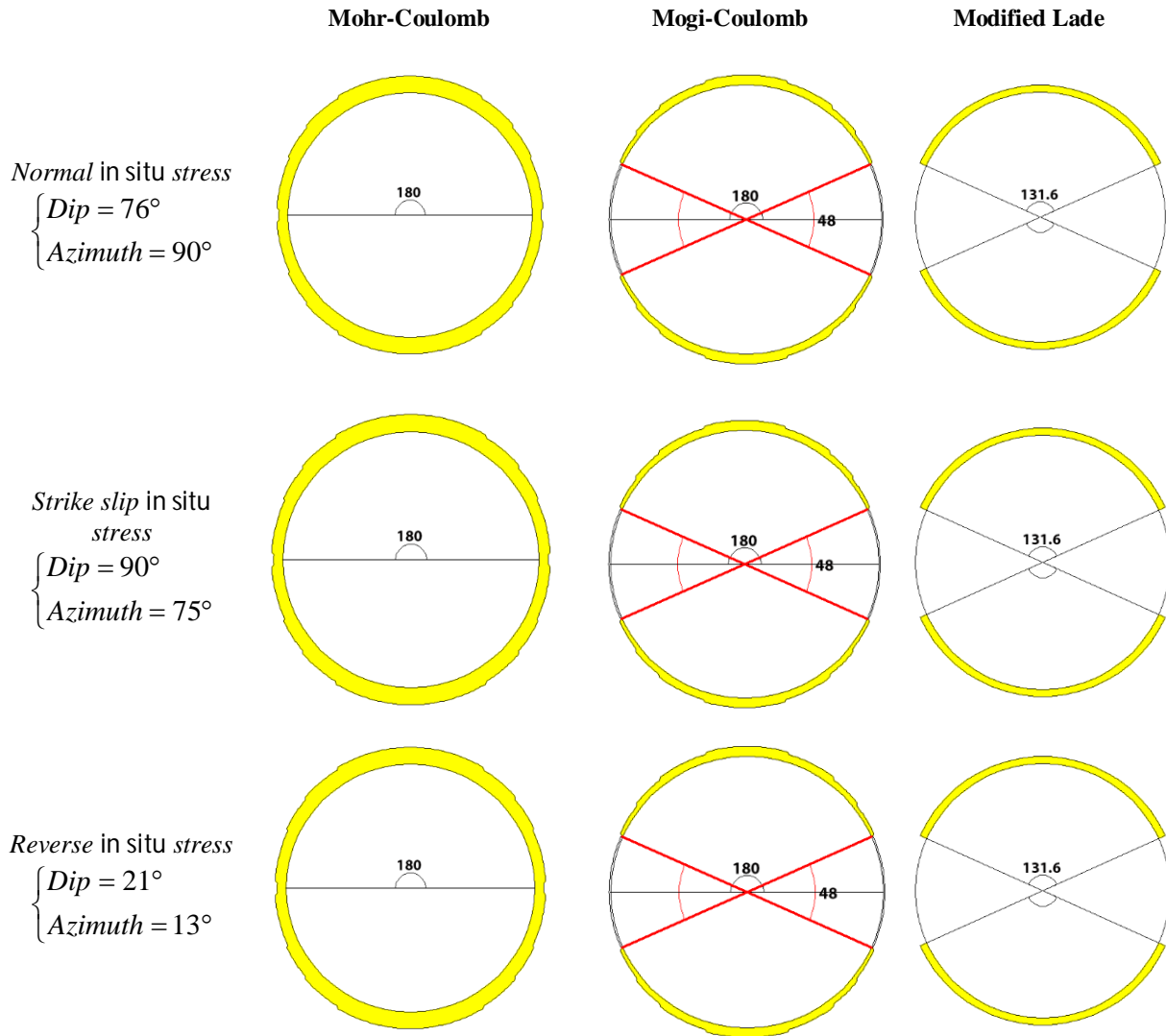


Figure 8. Final shape of the failure zone in the worst situation of the three *in-situ* stress regimes.

The finite difference numerical method can model borehole at different dips and arbitrary orientations. It can also predict the optimized mud weight window and well trajectory. Thus it was tried to estimate the extension of the plastic zone (failure zone) around the borehole wall with a specific trajectory to verify the aforementioned analytical method. In the model, a deviated well with a dip of 35° , a dip direction of 360° , and a diameter of 20 cm was analyzed under the normal *in-situ* stress regime. In order to avoid the boundary effect problems, and for a better presentation of the elastic-plastic behavior of the host rock, the dimensions of $4\text{ m} \times 4\text{ m} \times 3\text{ m}$ were considered for the model. As shown in Figure. 9, all sides and the bottom surface of the investigated 3D cube block

were fixed. The overburden stress was applied to the upper boundary of the block. According to Table 1, the far field stress, pore pressure, well pressure, and rock mechanics properties of the investigated example were applied to the model. After solving the model, an extension of the failure zone and distribution of the maximum and minimum principal stresses are shown as outputs of the software in Figures. 10 and 11. As illustrated in Figure 11, the extension of the failure zone has a width and a depth of 99° and 4.95 cm, respectively. Accordingly, the numerical model is in a good conformity with the analytical model, and the analytical model can be claimed to have enough credit.

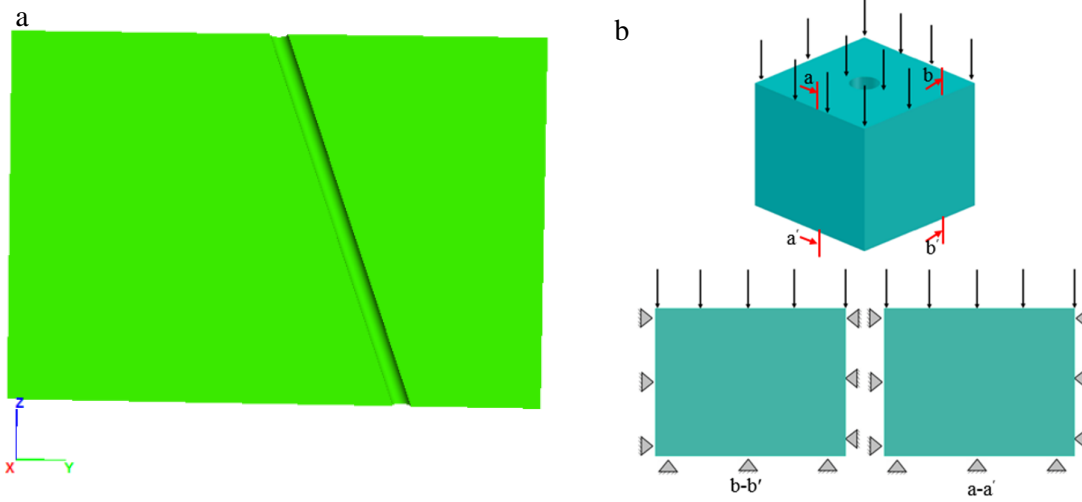


Figure 9. Geometry of the model a) cross-section of geometry of the model b) boundary condition of the model.

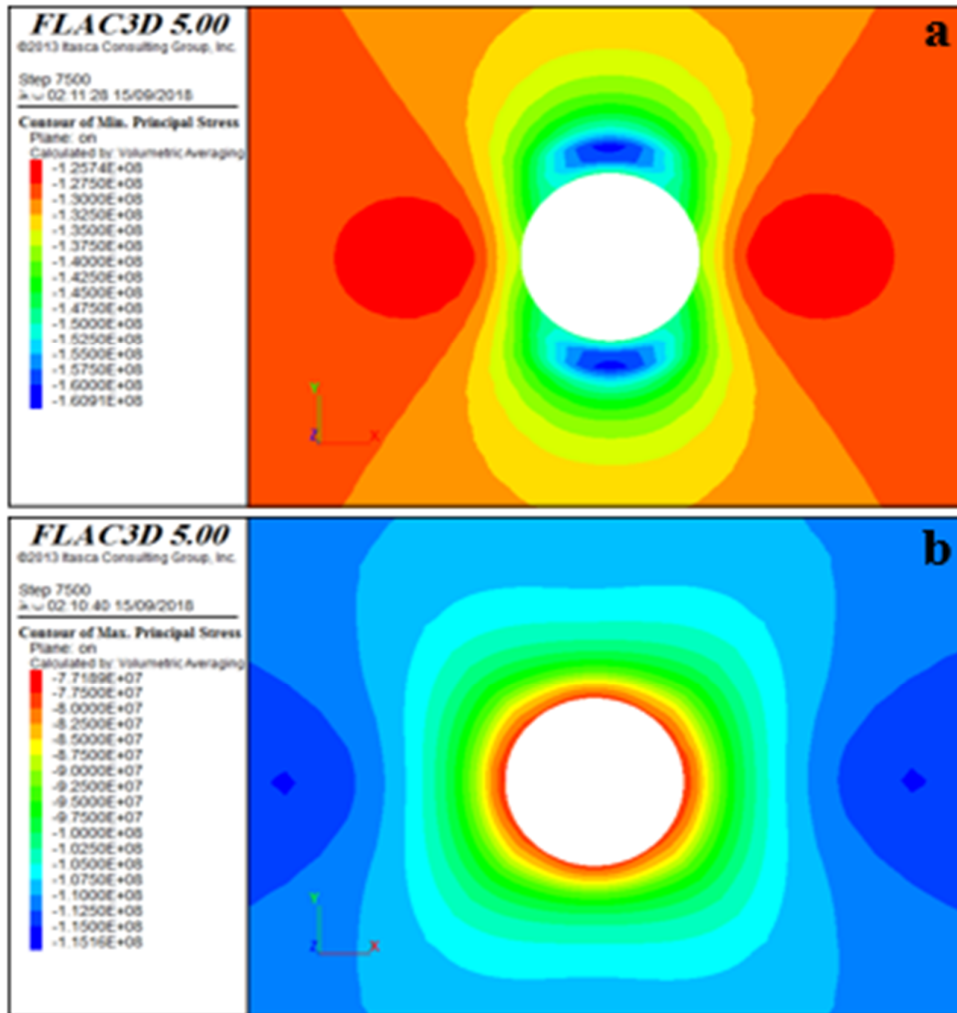


Figure 10. Condition of stress distribution around borehole wall at the validated example a) minimum principal stress b) maximum principal stress.

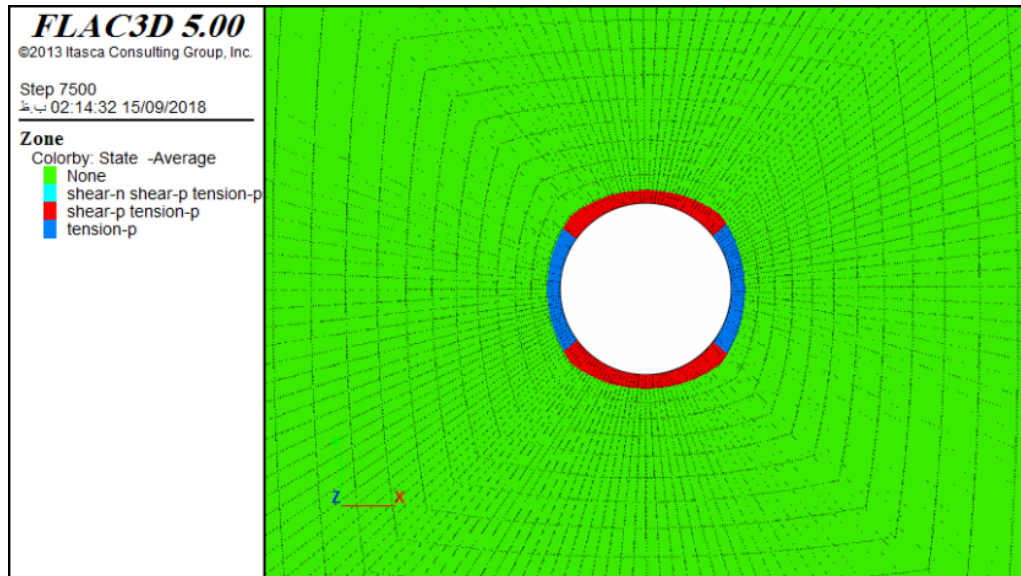


Figure 11. Extension of the plastic zone around the borehole wall at the validated example.

3. Results and discussion

A common difficulty encountered when working on geomechanics projects is data collection. Hence, the existence of a reliable and complete input data can have an important role in the success of each study. Proposing the optimum well trajectory in an Iranian oilfield SW of Iran was the main aim of this paper. In order to optimize the drilling path through each formation of the investigated oilfield, eight horizons were selected based on the formation sequence and rock samples. These samples were prepared from one borehole of the target oilfield. The required rock mechanics tests conducted on these samples consist of the triaxial test, uniaxial test, and Brazilian test. As shown in Table 2, the rock properties of the mentioned horizons are the result of the correlation between the rock mechanics tests with log data. This correlation is shown in Figure 12. The available log data during

this work can be seen in Figure 13. It should be noted that these rock mechanics samples were prepared based on the geomechanics unit of formations in the target borehole. According to the world stress map and the statistical analysis conducted in this field, the *in situ* stress can be claimed to be normal in the strike-slip stress regime. Also analysis of the FMI data and the orthogonal caliper indicated that the majority of these elliptical breakouts had their longer axis oriented in almost the N45W-S45E direction. Therefore, the orientation of the minimum horizontal stress can be reported to be almost N45W-S45E, and the orientation of the maximum horizontal stress is N45E-S45W. As illustrated in Figure 14, the magnitude of the *in situ* stress, pore pressure, and well pressure in any of the eight mentioned horizons are summarized in Table 3.

Table 2. Rock mechanical properties of the studied horizons.

Horizon	Depth (m)	Poisson's ratio	UCS (MPa)	C (MPa)	Φ°
1	2488	0.22	26.51	2.64	48
2	2650	0.17	39.5	6.22	55
3	2850	0.2	29.12	2.13	51
4	3150	0.17	27.36	5.80	46
5	3350	0.17	13.24	3.41	49
6	3500	0.16	22.7	1.22	52
7	3700	0.14	14.92	6.04	46
8	3973	0.17	12.24	14.3	54

Table 3. Stress distribution, pore pressure, and well pressure in each section.

Horizon	Depth (m)	Over-burden stress (MPa)	Maximum horizontal stress (MPa)	Minimum horizontal stress (MPa)	Pore pressure (MPa)	Well pressure (MPa)
1	2488	60.98	48.55	41.24	26.02	31.70
2	2650	64.70	53.65	44.74	27.71	34.36
3	2850	69.67	71.24	51.69	29.80	32.86
4	3150	76.94	56.37	49.70	32.94	40.70
5	3350	82.00	64.42	56.29	35.02	44.10
6	3500	85.58	66.14	57.70	36.60	46.19
7	3700	90.50	61.19	48.12	38.68	49.00
8	3973	98.64	84.61	75.42	54.26	75.70

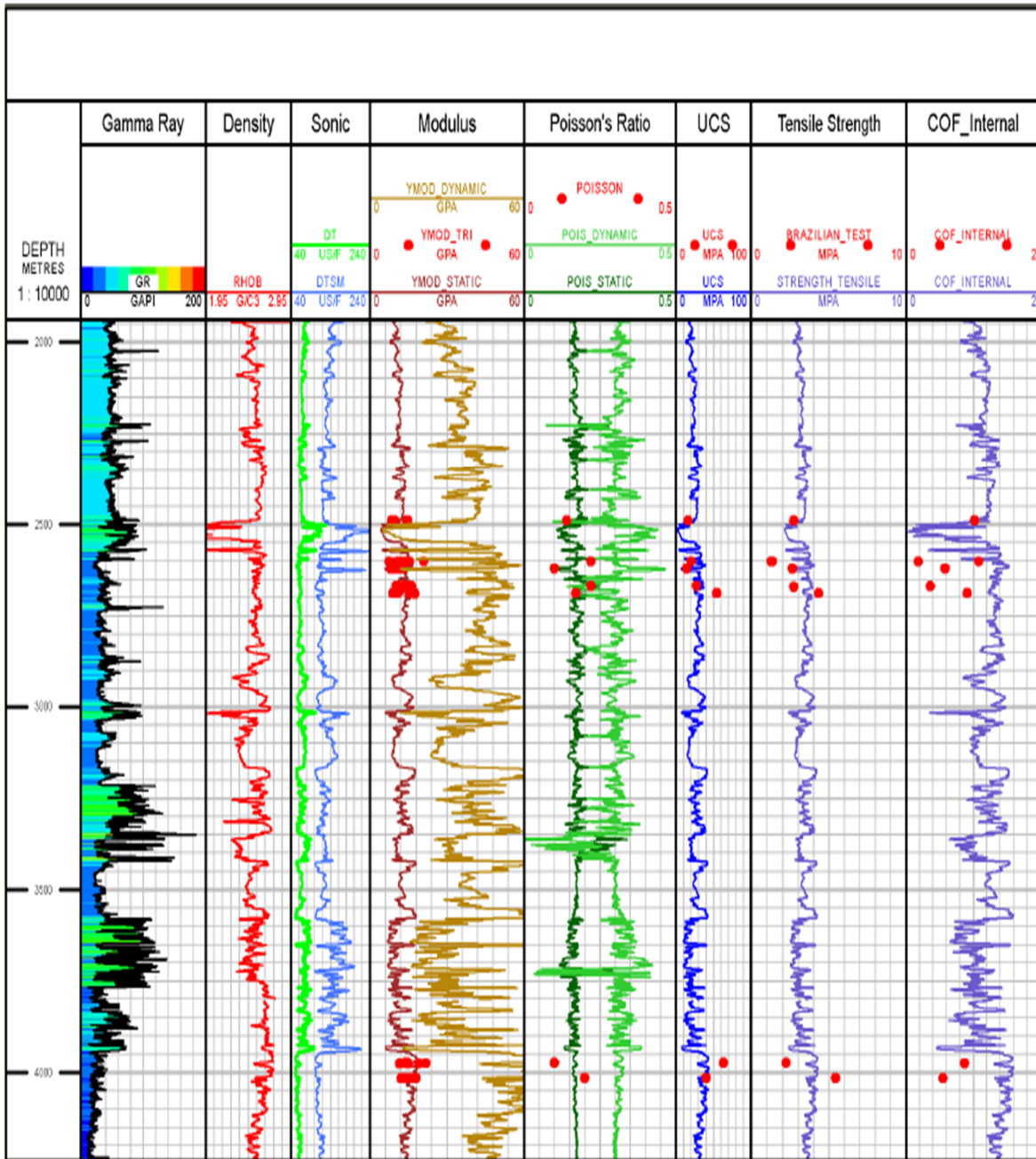


Figure 12. Correlation between the rock mechanic test and the log data.

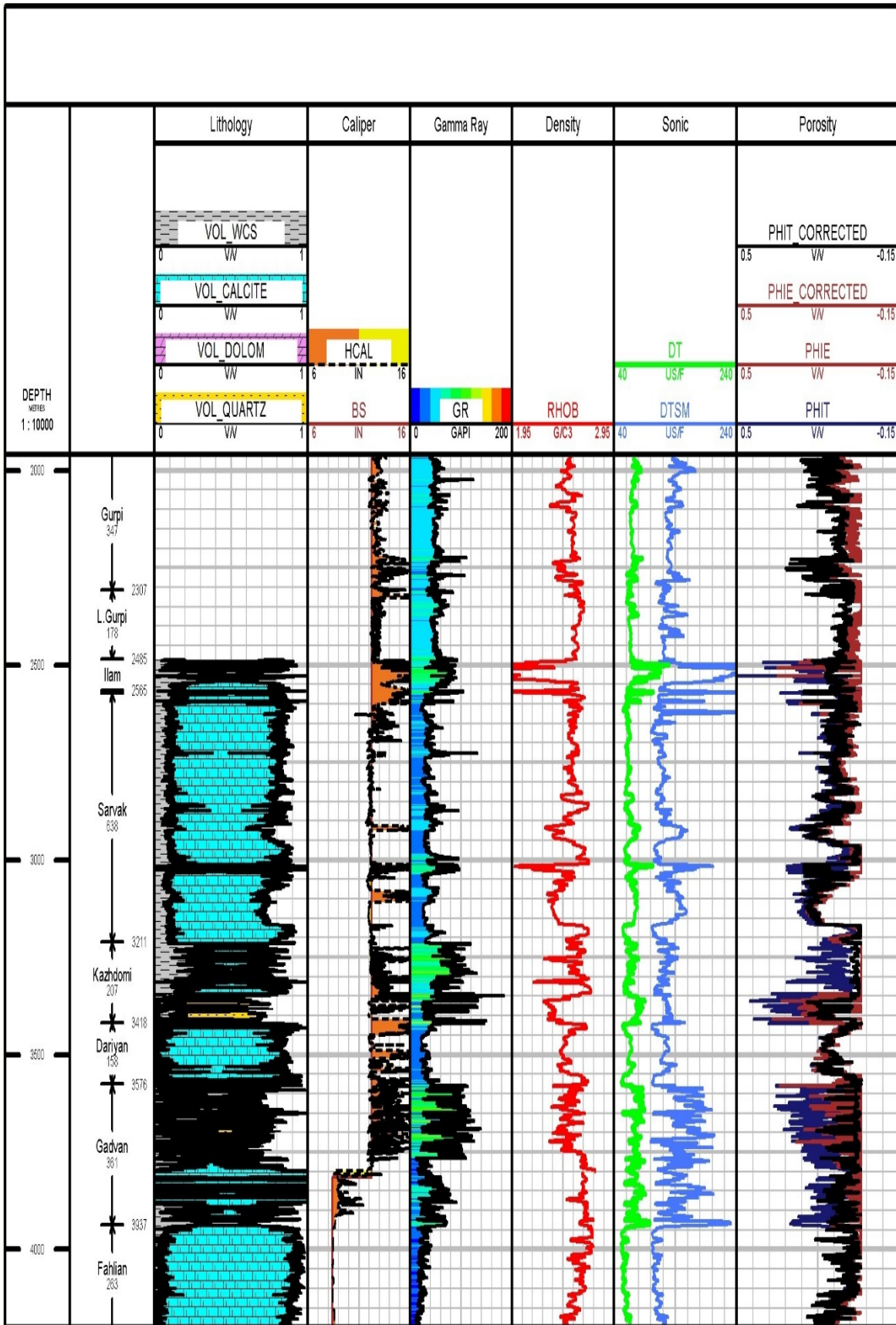


Figure 13. Raw log data from the candidate well.

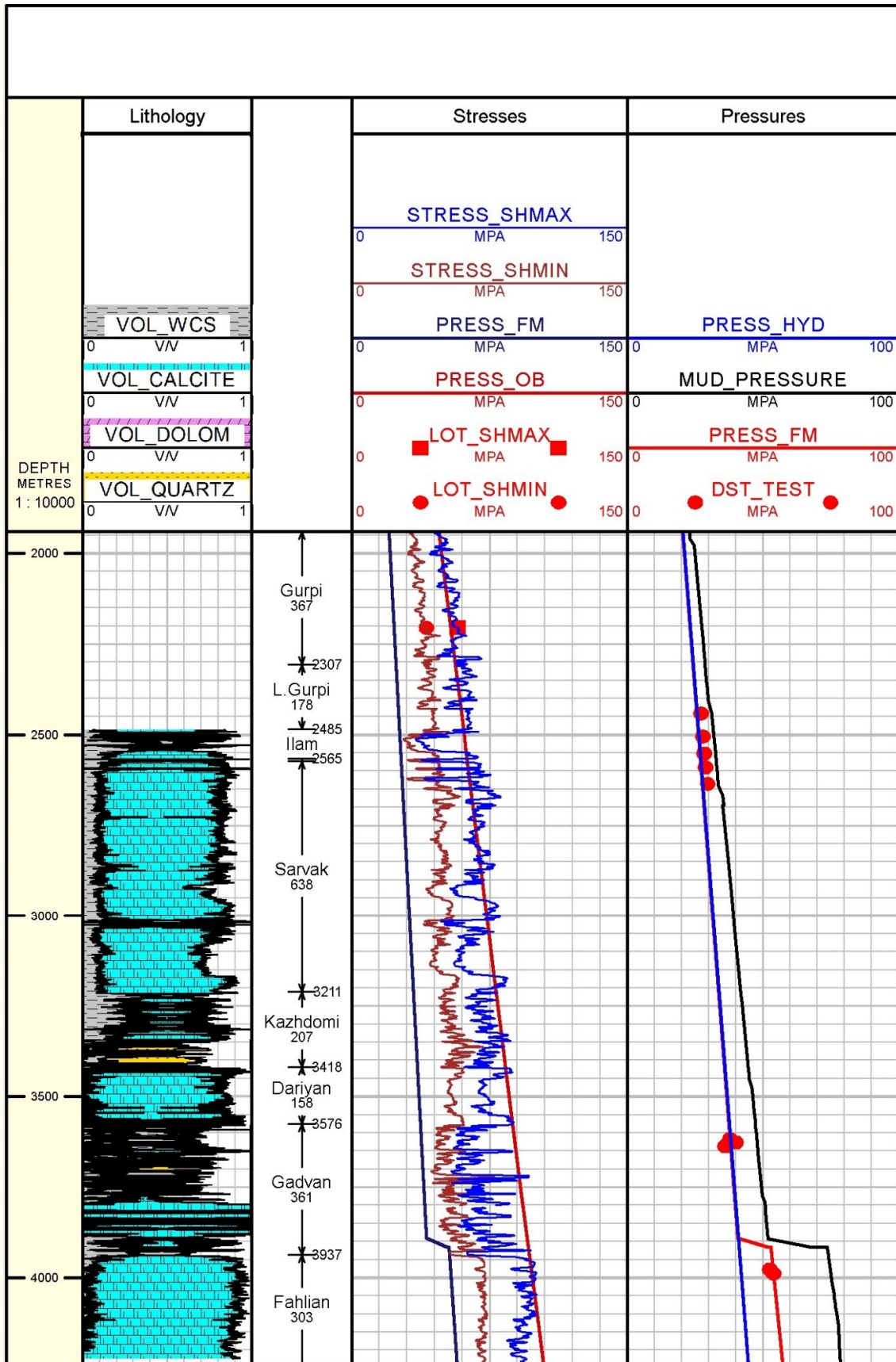


Figure 14. Stress profile of the candidate well.

3.1. Proposing optimum well trajectory candidate oilfield

As mentioned in Section 2.5.1, the optimized orientation by failure area and failure width is not in an acceptable agreement with the optimized orientation by the minimum mud pressure and failure depth. Also optimizing the well trajectory based on the failure area is more reasonable and logical. Therefore, the failure area, failure width, minimum mud pressure, and maximum mud pressure were selected to propose the most optimum and practical drilling path based on three failure criteria of Mohr-Coulomb, Mogi-Coulomb, and Modified Lade. The minimum and maximum mud pressures were used to suggest the safe mud window in each inclination and azimuth. With respect to the stress condition and rock properties of each mentioned horizons in Tables 2 and 3, the variation in the four suggested factors was analyzed in different orientations. Due to the numerous investigated horizons, the results of only two horizons of 2850 m and 3700 m are described in this section because among the target horizons, they are in the worst instability situation. The results of the other horizons can be seen in Appendix A.

The horizon of 2850 m is located in the Sarvak formation and follows the strike-slip stress regime. Variation in the maximum and minimum mud pressure, failure width, and relative failure area in this horizon along the arbitrary orientation are illustrated in Figure 15. With respect to this figure, for any well drilled along the maximum horizontal principal stress, extension of the failure zone is minimized. The failure width and relative failure area reach a critical value by drilling a highly deviated well ($\theta > 60^\circ$) or a horizontal well along the minimum horizontal principal stress. On the other hand, for a highly deviated ($\theta > 70^\circ$) and horizontal well along E-W, the minimum mud pressure is low and the mud window is in a safe zone. It should be noted that the variation in the minimum mud pressure with inclination and azimuth is limited to a specific and small range. Thus in this horizon, the mud pressure could not be proposed as a reliable prediction. Due to the extension of the failure zone with different orientations, the horizontal and deviated wells ($0^\circ < \theta < 90^\circ$) along the maximum horizontal principal stress are known as the safe drilling path. Another selected horizon is located in the Gadvan formation with a depth of 3700 m. The stress regime of this formation is normal. As illustrated in

Figure 16, no significant failure zone takes place in the arbitrary deviated well. Actually, under the current stress situation and rock properties, the critical failure zone will only appear along the highly deviated well with an inclination of 80° from the vertical well and azimuth of 105° to 155° . In this direction, based on the Mogi-Coulomb and modified Lade criteria, the relative failure area reaches %9 to %8, respectively. Only the Mohr-Coulomb criterion predicts %20 of the relative failure area in this orientation. The minimum and maximum mud pressure in different orientations offer the deviated well along the minimum horizontal *in-situ* stress (120° to 150° azimuth) with 60° deviation from the vertical well. Also a vertical and low-deviated well has an acceptable stability. Accordingly, none of the three failure criteria suggest the horizontal and highly deviated wells as a stable direction. With respect to the extension of the failure zone and variation in the maximum and minimum mud pressure in an arbitrary deviated well, drilling along the vertical and low deviated ($\theta < 60^\circ$) wells is known as the most stable direction of the Gadvan formation.

As it can be seen in Figures. A1 to A6, the remaining candidate horizons show the same variation in the mud pressure and failure zone along the arbitrary deviation of the well. The minimum and maximum mud pressures propose the vertical, deviated wells ($\theta < 45^\circ$) along the minimum principal stress. On the other hand, extension of the failure zone around the borehole wall can be claimed to be negligible in different orientations of these horizons. However, drilling a deviated well ($0^\circ < \theta < 60^\circ$) through any azimuth decreases the relative failure area and the failure width to a minimum amount. Generally, the critical mud pressure can be considered as the main factor for the optimization of the well trajectory of these horizons due to an unclear failure zone. Eventually, drilling the vertical and low deviated wells ($\theta < 45^\circ$) can be suggested as the optimum trajectory through the eight formations of the investigated oilfield (Figures 15 and 16 and Figures A1 to A6). The vertical direction comes as the first priority due to its simplicity. The safe mud window and amount of the relative failure area along the suggested well trajectory are shown in Figure 17. On the other hand, the Mohr-Coulomb criterion has a more conservative prediction than the other two failure criteria. Mogi-Coulomb and modified Lade propose more reliable and realistic results but Mogi-Coulomb is more user-friendly.

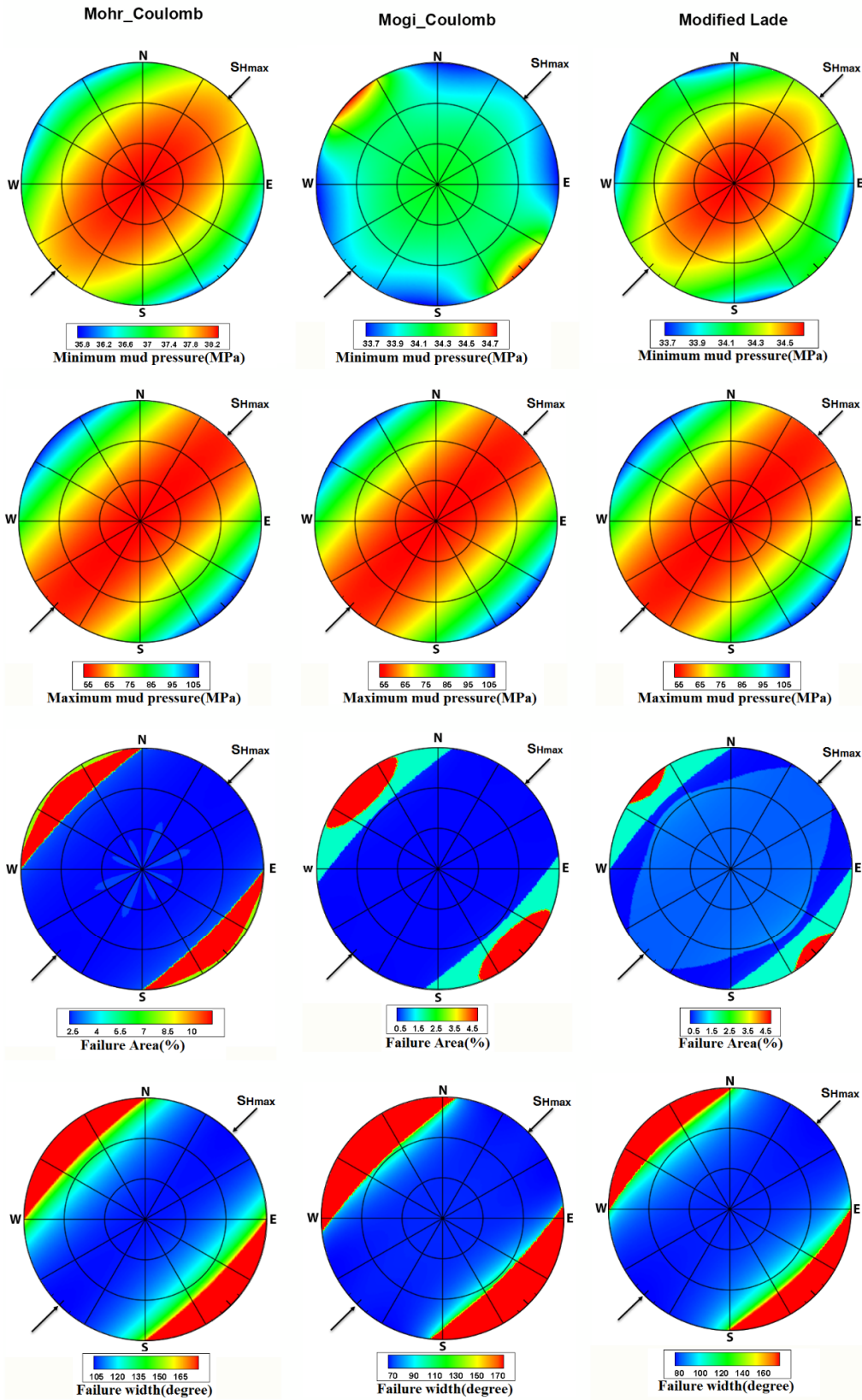


Figure 15. Stability of arbitrary wellbores under different failure criteria in at depth of 2850 m.

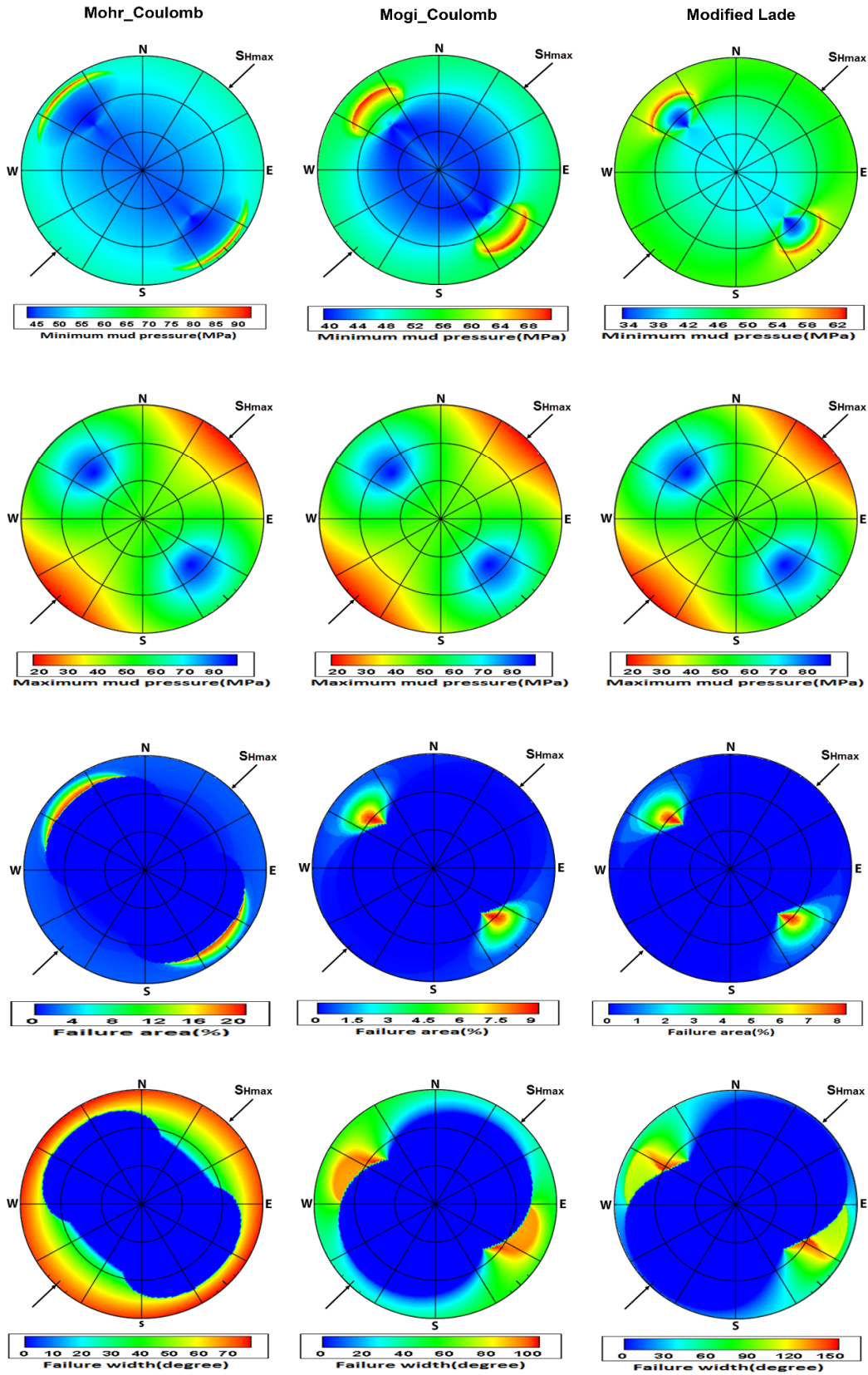


Figure 16. Stability of arbitrary wellbores under different failure criteria in a depth of 3700 m.

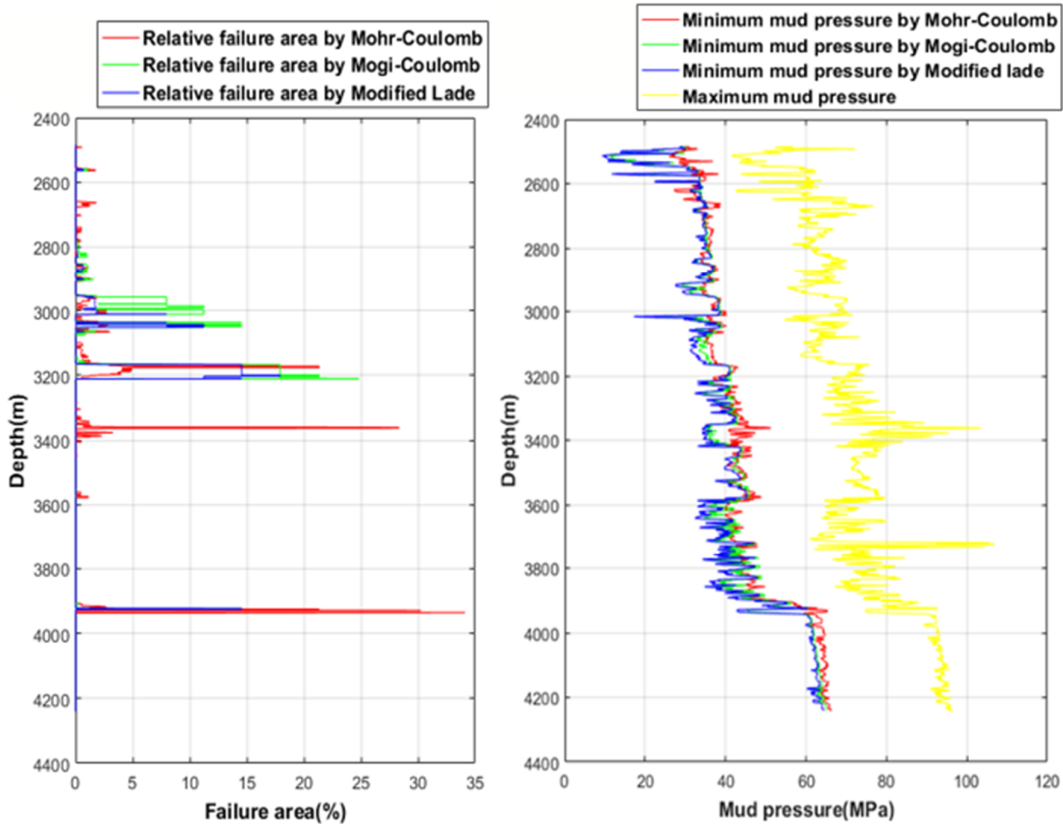


Figure 17. Safe mud window and relative area of failure zone in the suggested drilling path.

4. Conclusions

In this work, it was tried to propose the most stable and optimum drilling path in an oilfield in Iran. The minimum and maximum mud pressure, relative failure area, and failure width were the key parameters of this work. In order to achieve this goal, eight horizons were selected with the help of the rock properties and stress condition of the investigated formations. Then the induced stresses were estimated in arbitrary orientations and substituted in the selected failure criteria. The mud pressures and failure zones obtained were presented by several stereonet graphs to determine the best well trajectory. As informed before, the minimum mud pressure, failure depth, failure width, and relative failure area may be used to predict breakout. The results obtained may be categorized into two groups. Group A includes the minimum mud pressure and failure depth, and group B includes the failure width and relative failure area. The results of the group A members are in more agreement as well as the results of group B for its members. Comparing groups A and B with the field data shows that group B can predict a better breakout orientation in various wellbore trajectories. Actually, the failure area presents a

more comprehensive and more economical stability analysis in comparison with the failure width and failure depth. Also it can play an important role in the other petroleum geomechanics studies such as sand production. However, it should be noted that only the bulky failure zone could cause a geomechanics problem. In most of the investigated horizons, the failure zone did not appear significantly around the borehole wall of any arbitrary deviation. Therefore, the variation in the mud pressure was selected as the main factor to optimize the drilling path. Finally, the vertical and low deviated ($\theta < 45^\circ$) drilling path was suggested as a stable and optimum direction. Furthermore, it should be noted that optimization of the well trajectory based on the failure zone may be considered as an acceptable method if considerable failure zone takes place around the borehole wall.

5. Reference

[1]. Bradley, W.B. (1979). Failure of inclined boreholes.
 [2]. Khatibi, S., Aghajanjpour, A., Ostadhassan, M. and Farzay, O. (2018). Evaluating Single-Parameter parabolic failure criterion in wellbore stability analysis.

Journal of Natural Gas Science and Engineering, 50, 166-180.

[3]. Ma, Y. and Yu, R. (2019). New analytical methods to evaluate uncertainty of wellbore stability. Journal of Petroleum Science and Engineering, 180, 268-277.

[4]. Ding, Y., Luo, P., Liu, X. and Liang, L. (2018). Wellbore stability model for horizontal wells in shale formations with multiple planes of weakness. Journal of Natural Gas Science and Engineering, 52, 334-347.

[5]. Albooyeh, M., Kivi, I.R. and Ameri, M. (2018). Promoting wellbore stability in active shale formations by water-based muds: A case study in Pabdeh shale, Southwestern Iran. Journal of Natural Gas Science and Engineering, 56, 166-174.

[6]. Albooyeh, M., Kivi, I.R. and Ameri, M. (2018). Promoting wellbore stability in active shale formations by water-based muds: A case study in Pabdeh shale, Southwestern Iran. Journal of Natural Gas Science and Engineering, 56, 166-174.

[7]. Li, Y. and Weijermars, R. (2019). Wellbore stability analysis in transverse isotropic shales with anisotropic failure criteria. Journal of Petroleum Science and Engineering, 176, 982-993.

[8]. Li, X., Jaffal, H., Feng, Y., El Mohtar, C. and Gray, K.E. (2018). Wellbore breakouts: Mohr-Coulomb plastic rock deformation, fluid seepage, and time-dependent mudcake buildup. Journal of Natural Gas Science and Engineering, 52, 515-528.

[9]. Han, Y., Liu, C., Phan, D., AlRuwalli, K. and Abousleiman, Y. (2019, March). Advanced Wellbore Stability Analysis for Drilling Naturally Fractured Rocks. In SPE Middle East Oil and Gas Show and Conference. Society of Petroleum Engineers.

[10]. Zoback, M.D. (2010). Reservoir geomechanics. Cambridge University Press.

[11]. Li, Q. and Tang, Z. (2016). Optimization of wellbore trajectory using the initial collapse volume. Journal of Natural Gas Science and Engineering, 29, 80-88.

[12]. Moraveji, M.K., Sabah, M., Shahryari, A. and Ghaffarkhah, A. (2017). Investigation of drill pipe rotation effect on cutting transport with aerated mud using CFD approach. Advanced Powder Technology, 28(4), 1141-1153.

[13]. Dijejin, Z.A., Ghaffarkhah, A., Sadeghnejad, S. and Sefti, M.V. (2019). Effect of silica nanoparticle size on the mechanical strength and wellbore plugging performance of SPAM/chromium (III) acetate nanocomposite gels. Polymer Journal, 51(7), 693-707.

[14]. Al-Ajmi, A.M. and Zimmerman, R.W. (2009). A new well path optimization model for increased mechanical borehole stability. Journal of Petroleum Science and Engineering, 69(1-2), 53-62.

[15]. Heidarian, M., Jalalifar, H., Schaffie, M. and Jafari, S. (2014). New analytical model for predicting the unstable zone around the borehole. SPE Journal, 19(06), 1-177.

[16]. Nasiri A, Ghaffarkhah A, Moraveji MK, Gharbanian A, Valizadeh M. Experimental and field test analysis of different loss control materials for combating lost circulation in bentonite mud. Journal of Natural Gas Science and Engineering. 2017 Aug 1; 44:1-8.

[17]. He, S., Zhou, J., Chen, Y., Li, X. and Tang, M. (2017). Research on wellbore stress in under-balanced drilling horizontal wells considering anisotropic seepage and thermal effects. Journal of Natural Gas Science and Engineering, 45, 338-357.

[18]. Wang, W., Wen, H., Jiang, P., Zhang, P., Zhang, L., Xian, C. and Xie, Q. (2019, March). Application of Anisotropic Wellbore Stability Model and Unconventional Fracture Model for Lateral Landing and Wellbore Trajectory Optimization: A Case Study of Shale Gas in Jingmen Area, China. In International Petroleum Technology Conference. International Petroleum Technology Conference.

[19]. Smart, E.G.D., Somerville, J.M. and MacGregor, K.J. (1991, January). The prediction of yield zone development around a borehole and its effect on drilling and production. In The 32nd US Symposium on Rock Mechanics (USRMS). American Rock Mechanics Association.

[20]. Behnia, M., Goshtasbi, K., Marji, M.F. and Golshani, A. (2014). Numerical simulation of crack propagation in layered formations. Arabian Journal of Geosciences, 7(7), 2729-2737.

[21]. Abdollahipour, A., Marji, M.F., Bafghi, A.Y. and Gholamnejad, J. (2015). Simulating the propagation of hydraulic fractures from a circular wellbore using the Displacement Discontinuity Method. International Journal of Rock Mechanics and Mining Sciences, 80, 281-291.

[22]. Jia, L., Chen, M., Jin, Y. and Jiang, H. (2017). Numerical simulation of failure mechanism of horizontal borehole in transversely isotropic shale gas reservoirs. Journal of Natural Gas Science and Engineering, 45, 65-74.

[23]. Yousefian H, Soltanian H, Marji MF, Abdollahipour A, Pourmazaheri Y. Numerical simulation of a wellbore stability in an Iranian oilfield utilizing core data. Journal of Petroleum Science and Engineering. 2018 Sep 1;168:577-92.

[24]. Aadnoy, B. S. and Kaarstad, E. (2010, January). History model for sand production during depletion. In SPE EUROPEC/EAGE Annual Conference and Exhibition. Society of Petroleum Engineers.

[25]. Wang, Z. and Gao, D. (2016). Multi-objective optimization design and control of deviation-correction

trajectory with undetermined target. *Journal of Natural Gas Science and Engineering*, 33, 305-314.

[26]. Zhang, W., Gao, J., Lan, K., Liu, X., Feng, G. and Ma, Q. (2015). Analysis of borehole collapse and fracture initiation positions and drilling trajectory optimization. *Journal of Petroleum Science and Engineering*, 129, 29-39.

[27]. Atashnezhad A, Wood DA, Fereidounpour A, Khosravianian R. Designing and optimizing deviated wellbore trajectories using novel particle swarm algorithms. *Journal of Natural Gas Science and Engineering*. 2014 Nov 1;21:1184-204.

[28]. Alkamil, E.H., Abbood, H.R., Flori, R.E. and Eckert, A. (2017, March). Wellbore stability evaluation for Mishrif formation. In *SPE Middle East Oil & Gas Show and Conference*. Society of Petroleum Engineers.

[29]. Fjar, E., Holt, R.M., Raaen, A.M., Risnes, R. and Horsrud, P. (2008). *Petroleum related rock mechanics*. Elsevier.

[30]. Goodman, R. E. (1989). *Introduction to rock mechanics* (Vol. 2). New York: Wiley.

[31]. Djurhuus, J. and Aadnoy, B.S. (2001, January). In-situ stress state from inversion of fracturing data from oil wells. In *DC Rocks 2001, The 38th US Symposium*

on Rock Mechanics (USRMS). American Rock Mechanics Association.

[32]. Aadnoy, B. and Looyeh, R. (2019). *Petroleum rock mechanics: drilling operations and well design*. Gulf Professional Publishing.

[33]. Aadnoy, B. and Looyeh, R. (2019). *Petroleum rock mechanics: drilling operations and well design*. Gulf Professional Publishing.

[34]. Rahimi, R. (2014). The effect of using different rock failure criteria in wellbore stability analysis.

[35]. Mogi, K. (1971). Fracture and flow of rocks under high triaxial compression. *Journal of Geophysical Research*, 76(5), 1255-1269.

[36]. Al-Ajmi, A. and Zimmerman, R. (2005). Wellbore stability analysis using the Mogi-Coulomb failure criterion.

[37]. Lade, P.V. (1977). Elasto-plastic stress-strain theory for cohesionless soil with curved yield surfaces. *International journal of solids and structures*, 13(11), 1019-1035.

[38]. Ewy, R.T. (1998, January). Wellbore stability predictions using a modified Lade criterion. In *SPE/ISRM Rock Mechanics in Petroleum Engineering*. Society of Petroleum Engineers.

Appendix A

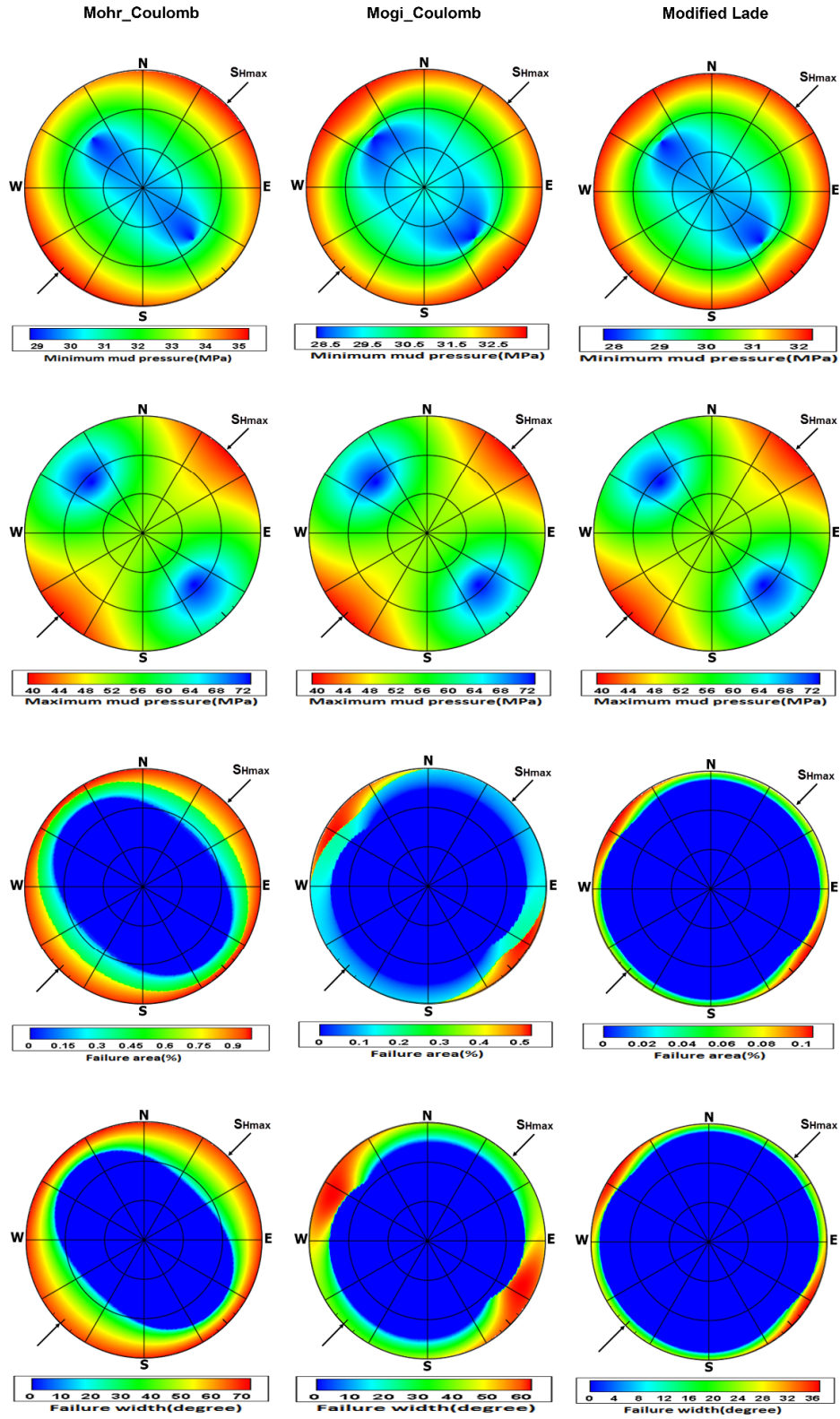


Figure A1. Stability of the arbitrary wellbores under different failure criteria in a depth of 2488 m.

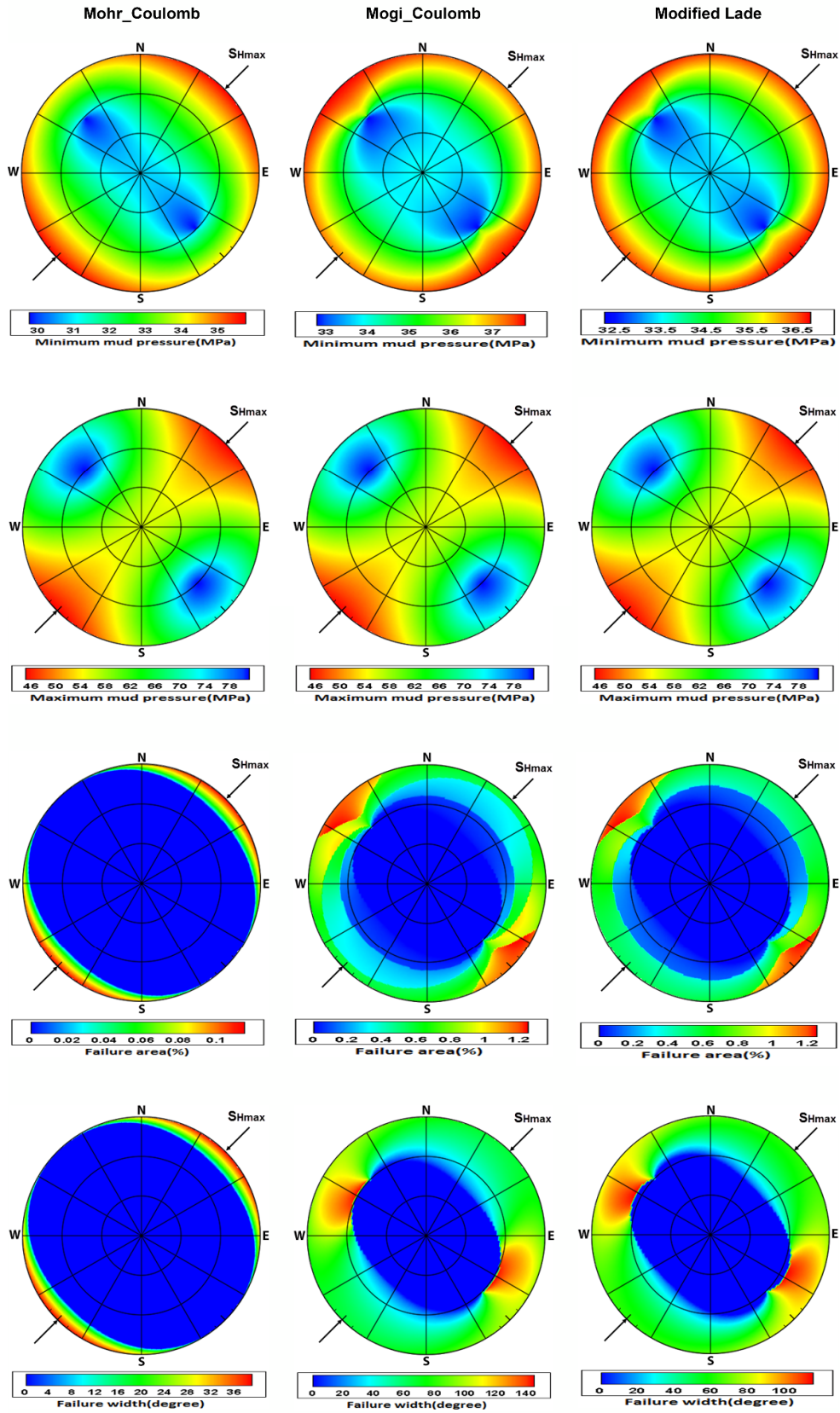


Figure A2. Stability of the arbitrary wellbores under different failure criteria in a depth of 2650 m.

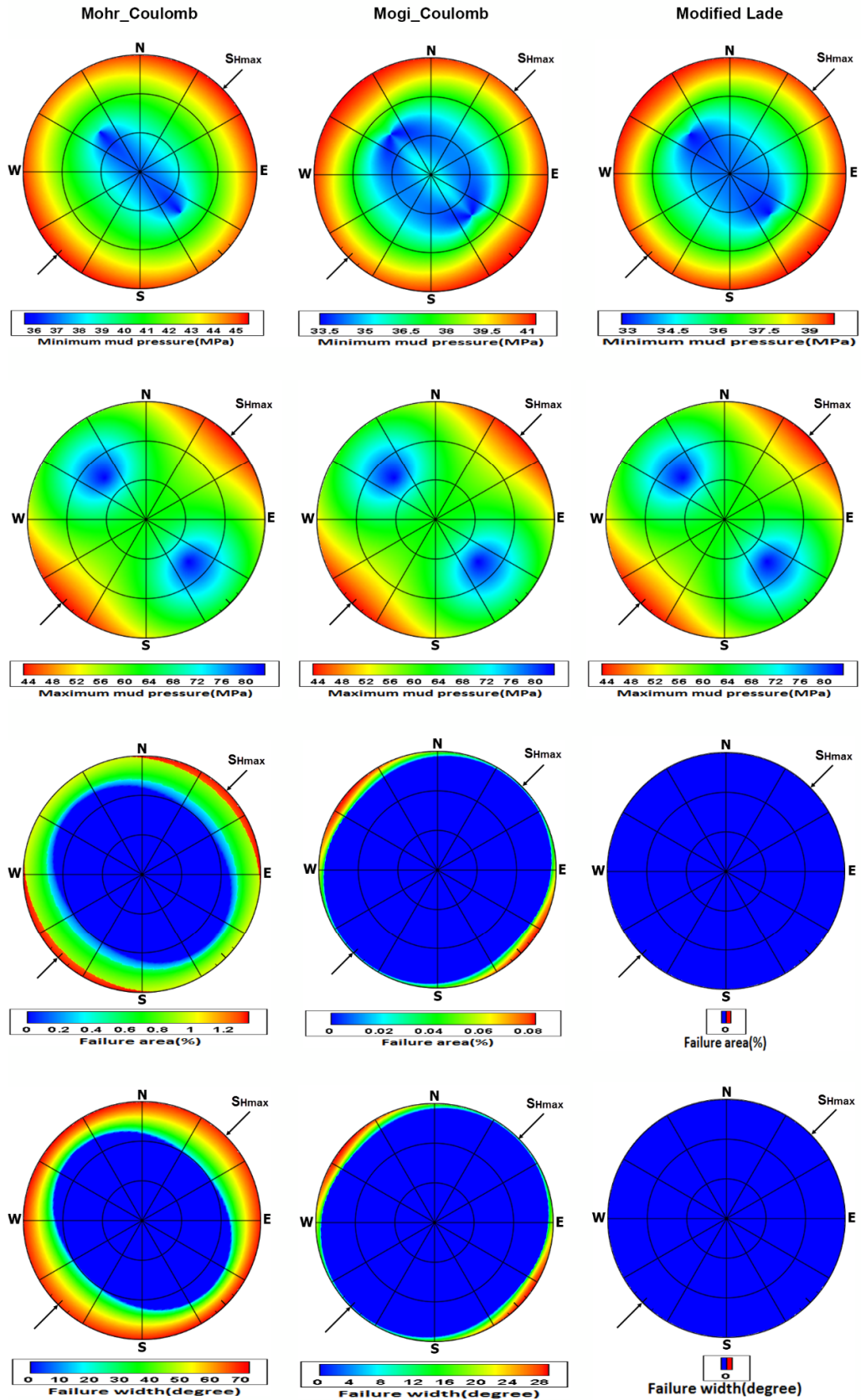


Figure A3. Stability of the arbitrary wellbores under different failure criteria in a depth of 3150 m.

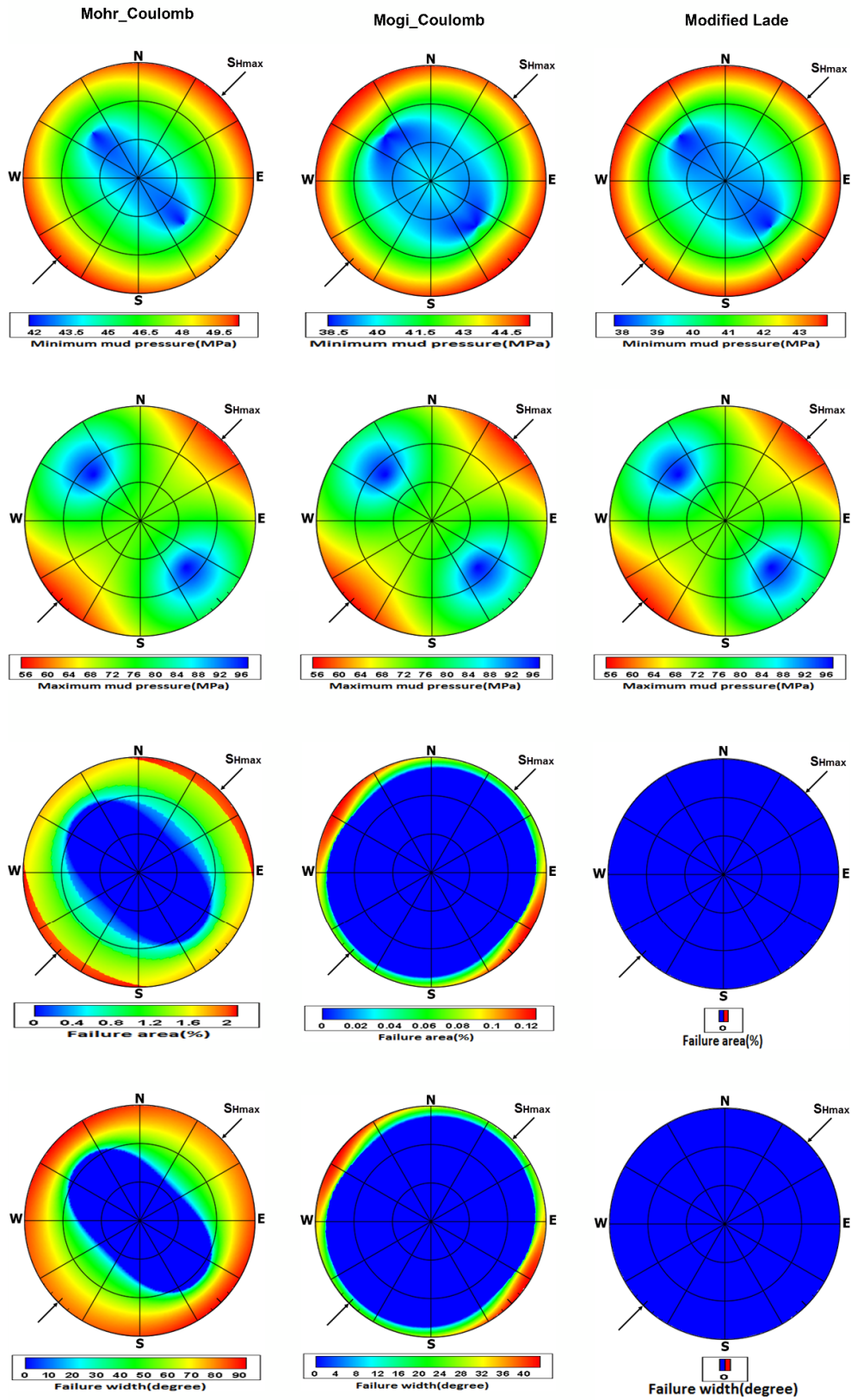


Figure A4. Stability of the arbitrary wellbores under different failure criteria in a depth of 3350 m.

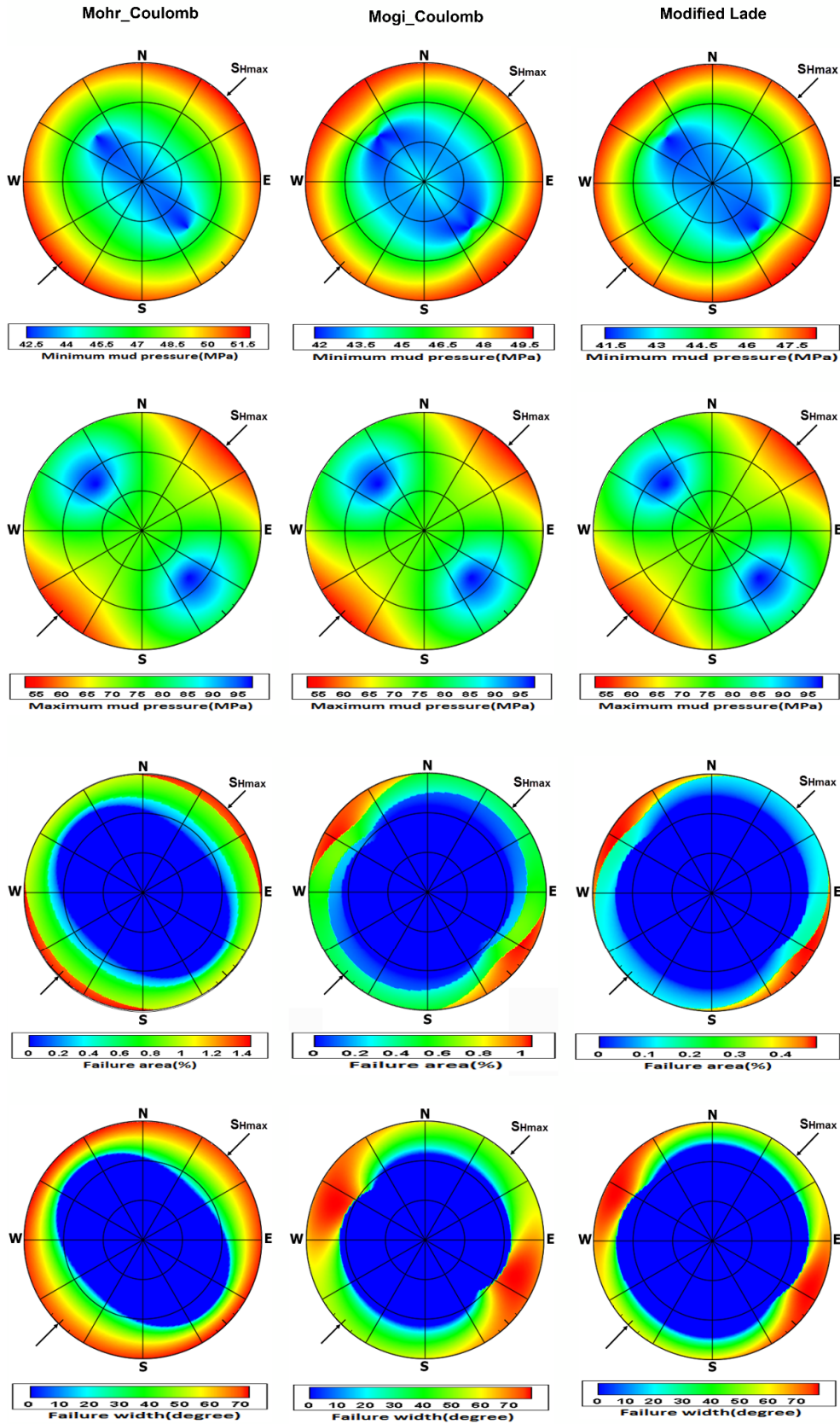


Figure A5. Stability of the arbitrary wellbores under different failure criteria in a depth of 3500 m.

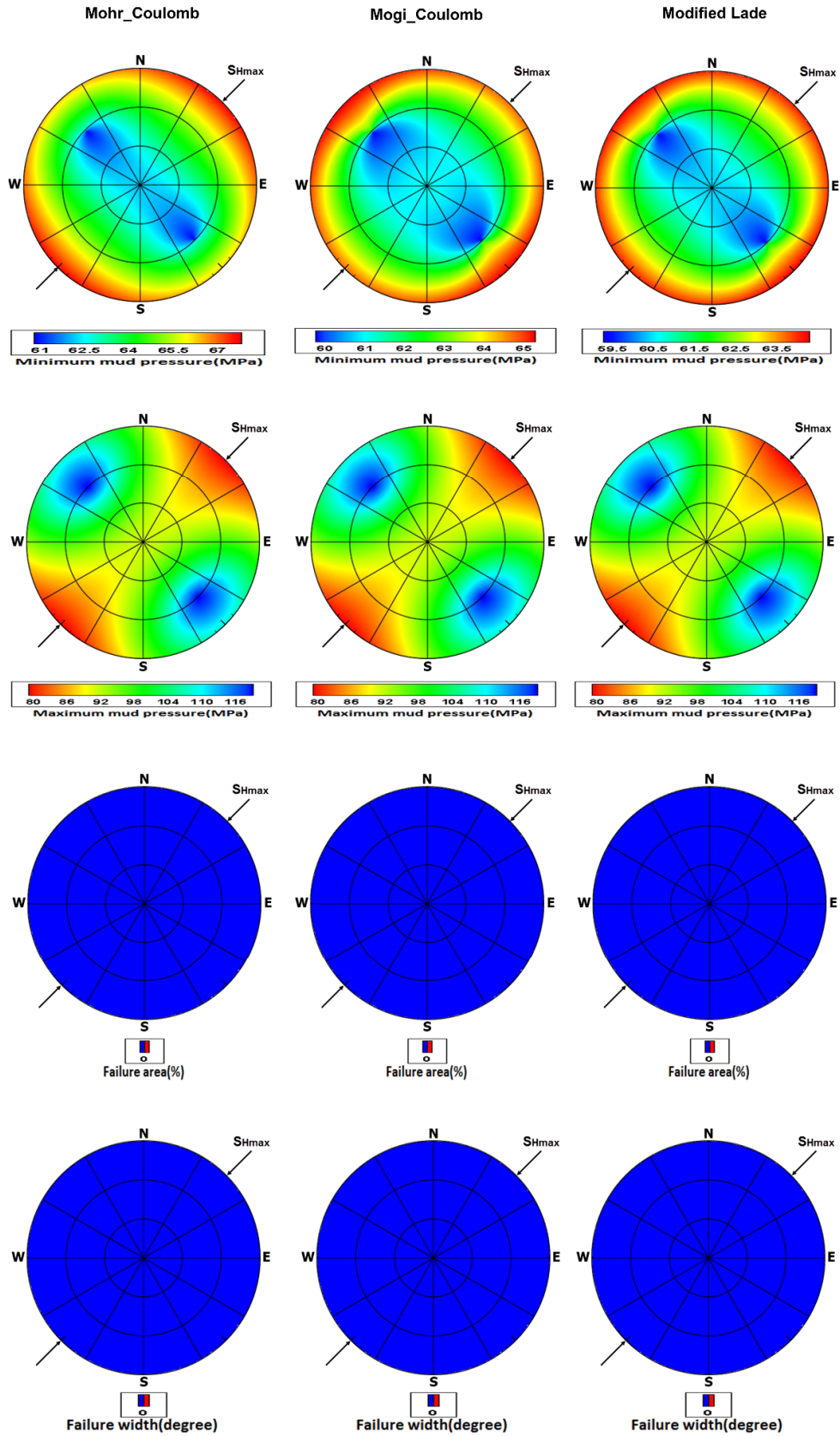


Figure A6. Stability of the arbitrary wellbores under different failure criteria in a depth of 3973 m.

بهینه سازی راستای حفاری یکی میادین نفتی ایران با استفاده از مفهوم فشار گل و ناحیه پلاستیک

هاتف یوسفیان¹، محمد فاتحی مرجی^{2*}، حمید سلطانیان¹، ابوالفضل عبداللهی پور³، یاسر پورمظاهری¹

1. گروه تکنولوژی‌های حفاری و تکمیل چاه پژوهشگاه صنعت نفت، تهران، ایران

2. دانشکده مهندسی معدن و متالورژی دانشگاه یزد، یزد، ایران

3. دانشکده مهندسی معدن دانشگاه تهران، تهران، ایران

تاریخ ارسال: 2019/8/12 تاریخ پذیرش: 2020/1/10

* نویسنده مسئول مکاتبات: mfatehi@yazd.ac.ir

چکیده:

همواره تخمین ناحیه شکست در پیرامون دیواره چاه یکی از مطالعات کاربردی پایداری چاه محسوب می‌شده است. از طرفی فشار گل نمی‌تواند به عنوان یک پارامتر مناسب در بهینه سازی راستای حفاری محسوب شود. چرا که فشار گل تنها قادر است احتمال و پتانسیل وقوع شکست را پیش بینی کند. از این‌رو در این تحقیق سعی شده است تا در ابتدا وضعیت گسترش ناحیه شکست در پیرامون دیواره چاه‌های با جهت‌داری متفاوت در شرایط رژیم تنش‌های مختلف بررسی شود. با فرض شرایط کرنش صفحه‌ای، معیارهای شکست موهر-کولمب، موگی-کولمب و لید اصلاح شده به عنوان معیارهای شکست مینا انتخاب شده‌اند. به عبارتی در تحقیق سعی شده است تا با استفاده از یکسری روابط تحلیلی، راستای بهینه حفاری یکی از میادین نفتی ایران به کمک مفهوم گسترش ناحیه شکست مورد ارزیابی قرار بگیرد. لذا به منظور پیش‌بینی میزان گسترش ناحیه شکست در پیرامون دیواره چاه، موقعیت وقوع شکست، گسترش عرضی ناحیه شکست و عمق ناحیه شکست در چاه‌های با جهت‌داری‌های مختلف تخمین زده شده است. سپس یک مدل جدید به منظور محاسبه گسترش ناحیه شکست پیرامون دیواره چاه‌های با جهت‌داری‌های مختلف ارائه شده است. به عبارتی مفهوم ناحیه شکست قادر است تا پایداری دیواره چاه را با بازده‌ای بیشتر و بهینه‌تر ارزیابی کند. نتایج به دست آمده از این تحقیق نشان می‌دهد که در میدان هدف، حفر چاه‌های قائم یا با آزیموت کمتر 45 درجه به عنوان راستای بهینه حفاری محسوب می‌شود. علاوه بر این، مطابق با نتایج به دست آمده می‌توان اذعان نمود که بهینه سازی راستای حفاری براساس مفهوم گسترش ناحیه شکست تنها در حالتی مناسب خواهد بود که میزان گسترش ناحیه شکست در پیرامون دیواره چاه قابل توجه باشد.

کلمات کلیدی: شکستگی‌های برشی پیرامون دیواره چاه، راستای حفاری، ناحیه شکست، فشار بحرانی، تنش القایی.